

Orbits in a Molecule. A Novel Way of Stereochemistry Through the Concepts of Coset Representations and Sphericities (Part 1)

Shinsaku Fujita

Department of Chemistry and Materials Technology,

Kyoto Institute of Technology,

Matsugasaki, Sakyo, Kyoto 606-8585, Japan

E-mail: fujitas@chem.kit.ac.jp

(Received April 13, 2005)

Abstract

The present series is devoted to a diagrammatical introduction to the USCI (unit-subduced-cycle-index) approach developed by Fujita (S. Fujita, "Symmetry and Combinatorial Enumeration in Chemistry", Springer-Verlag, 1991). In Part 1 of this series, intramolecular stereochemistry is discussed by emphasizing *orbits* as sets of symmetry-equivalent objects. In particular, concurrent appearance of orbits of various kinds in a molecule is discussed diagrammatically, where any orbits are shown to be controlled by three kinds of sphericity indices (a_d , c_d , and b_d) correlated to coset representations (CRs). Derivation of molecules of given symmetries is discussed in terms of concurrent desymmetrization of orbits, where USCI-CFs (unit subduced cycle indices with chirality fittingness) are obtained diagrammatically as products of sphericity indices. The concurrent behaviors of orbits are explained by using a regular body, the positions of which are segmented in terms of segmentation patterns so as to give segmented regular bodies. Such segments are studied as models of ligands or proligands so that segmented regular bodies can be regarded as models of three-dimensional molecules (stereoisomers). The segmented regular bodies are used to generate

CRs and to derive subductions of CRs diagrammatically. The generality of the procedure is confirmed so as to be capable of generating the subduction table, the USCI-CF table, the USCI table, and the mark table of \mathbf{D}_{2d} -point group, which have been alternatively obtained and used in the Fujita's USCI approach. Diagrammatical correspondence between segments and cosets are examined in detail so that the relationship between subduction of CRs and double cosets is clearly demonstrated. Several terms (e.g., *regular bodies*, *segments*, *segmentation patterns*, *transformulas*, and *assemblies of transformulas*) are introduced in order to give succinct but strict foundations to the present diagrammatical approach. It is concluded that *any symmetrical properties appear in regular bodies*.

1 Introduction

Stereoisomerism among molecules (intermolecular stereochemistry) and stereochemistry in molecule (intramolecular stereochemistry) are intimately related to each other, as implied by the parallelism of their terminology:

1. The word "stereoisomer" or "stereoisomeric" for the stereoisomerism has two meanings. Thus, two stereoisomers are *different* in their geometrical configuration, while they are *equivalent* because they have the *same* connectivities between the atoms involved. The word "enantiomer" (subcategory of "stereoisomer") also has two meanings. Thus, (two) enantiomers are *different* in their geometrical configuration, while they are *equivalent* (superposable) by reflection (or rotoreflection strictly). For example, a tetrahedral molecule Cabcd (a, b, c, and d: atoms of different types) and its enantiomer are regarded as being different or being equivalent according to distinct viewpoints of discussions. Organic chemists tend to put emphasis on "difference" but not on "equivalence" in their discussions on stereoisomerism.
2. On the other hand, the word "enantiotopic" for the intramolecular stereochemistry has two meanings. Thus, two enantiotopic sites are *different* in their geometrical configuration, while they are *equivalent* (superposable) by reflection (or rotoreflection strictly). For example, the two a's in a tetrahedral molecule Ca₂bc are enantiotopic so that they are regarded as being different on the action of chiral reagents or as being equivalent because of reflective superposability. The word "stereoheterotopic" that was proposed to correspond to the word "stereoisomeric" [1] obviously puts emphasis on "difference". The lack of the standpoint "equivalence" in the conventional usage of the word "stereoheterotopic" has given a narrow prospect to organic chemists.

The conventional descriptive stereochemistry is deficient in a common theoretical framework for comprehending the parallelism between the intermolecular stereochemistry and the intramolecular one. In fact, most textbooks for organic [2, 3] and inorganic stereochemistry [4] have dealt with the items enumerated above in a rather separate manner. Although Mislow et al. pointed out the importance of local chirality [5, 6], their discussions have not been concerned with such a common theoretical framework.

Moreover, the conventional chemical combinatorics based on Pólya's theorem [7, 8] regards chemical compounds as graphs, not as three-dimensional (3D) chemical structures, so that it is incapable of counting stereoisomers properly, as pointed out in recent articles [9, 10]. Thus, the conventional chemical combinatorics cannot be successfully combined with the conventional descriptive stereochemistry because of the lack of such a common theoretical framework.

As found in the preceding paragraphs, the common theoretical framework to be developed should first comprehend the two aspects, i.e., the “difference” and the “equivalence”. Second, it should integrate the two fields, i.e., the intramolecular stereochemistry and the stereoisomerism. Third, it should harmonize the two disciplines, i.e., the descriptive stereochemistry (the intramolecular stereochemistry and the stereoisomerism) and the chemical combinatorics.

Fujita has proposed the concept of *sphericity* derived from *coset representations* (CRs) as a key concept for constructing the common theoretical framework [11], which is now referred to as the USCI (unit-subduced-cycle-index) approach [12]. Mathematically speaking, the USCI approach has accomplished the integration of point-group theory and permutation-group theory as well as the integration of linear-representation theory and permutation-representation theory in terms of the key concept *sphericity*, as discussed in a previous article [13]. Because the point-group theory and the linear-representation theory are concerned with continuous objects while the permutation-group theory and permutation-representation theory deal with discrete objects, the USCI approach provides us with a tool for discussing continuous objects and discrete objects in a common framework.¹ The concept has been successfully applied to various stereochemical problems, as summarized in recent account papers [15, 16].

The original proposal of the sphericity concept [11, 12], however, has been based on a mathematical definition of CRs so that it may cause some sense of bias or rejection to organic chemists. In fact, this situation was pointed out by Mead in his book review [17] on Fujita’s monograph on the USCI approach [12]: “Although the book is in principle self-contained, containing some introductory chapters on the fundamentals of group theory, it is really aimed at readers who already acquainted at least with the basic concepts of group theory and who are willing to think mathematically.” and “This book is not easy going, but the reader who makes the necessary effort will be rewarded by the acquisition of some powerful tools and deep insights. If the coming generation of chemists becomes as familiar with mark tables and their uses as the present generation is with character tables, much of the credit will go to Fujita and the present book”. Recently, the situation and related barriers to Fujita’s USCI approach were again referred to as an “*organic chemistry paradox*” in the “*Era of Fujita*” by El-Basil in his review reported in this journal [18].²

To avoid the difficult situation, a more intuitive definition of the concept has recently been developed by Fujita [21, 22], where a minimum set of knowledge on group theory is required. By following the intuitive definition, the importance of orbits and sphericity indices and that of local symmetries appearing in subductions of coset representations have been discussed for introductory courses of stereochemistry [23, 24]. Remaining tasks that should be pursued in the present series of articles are to demonstrate the effectiveness of the intuitive definition by using illustrative examples and to confirm the compatibility with the mathematical definition.

¹It should be noted that the term “orbit” in the title of this article is different from the term “orbital” used in quantum chemistry. According to the present context, the term “orbit” is concerned with discrete objects, while the term “orbital” is concerned with continuous objects. Mark tables for specifying “orbits” and character tables for specifying “orbitals” have been integrated by means of the concept of *markaracter tables* proposed by Fujita [14], where the term “markaracter” has been coined by combining “mark” and “character”.

²I (Fujita) underwent academic training as a synthetic organic chemist and I *am* an organic chemist, as I have recently published monographs entitled “Computer-Oriented Representation of Organic Reactions” [19] and “Organic Chemistry of Photography” [20]. Hence, the difficult situation has long given me a sense of frustration. Although most fundamental items of the sphericity concept have been already described in a general and somewhat mathematical fashion in my previous monograph “Symmetry and Combinatorial Enumeration in Chemistry” [12], I believe that the present article would be permissible to be published since it involves some additional viewpoints with illustrative examples for comprehending the concept.

The present article (Part 1) is devoted to “intramolecular stereochemistry” (stereochemistry in molecule), where the concept of sphericity works well in molecule. On the other hand, Part 2 will deal with “intermolecular stereochemistry” (stereoisomerism among molecules), where the concept also works well among molecules. Part 3 will demonstrate that the integration of the two aspects (Part 1 and Part 2) gives a basis of chemical combinatorics.

2 Orbits and Sphericities

The subjects of this section have once been discussed in a previous educational article [23], where methane derivatives have been used as examples. Here, they are restated by using allene derivatives because the allene derivatives will be adopted as common examples throughout the present series.

2.1 Intuitive Definitions

Any objects (e.g., atoms and bonds) in a molecule can be categorized into sets of equivalent objects. Such sets are called *orbits* or *equivalence classes*, where the number of members is called *the size of the orbit*. For example, the four hydrogen atoms in an allene molecule of D_{2d} -symmetry (**1** or **2**) are equivalent to give a four-membered orbit, the two terminal carbon atoms on the C=C=C axis are equivalent to give a two-membered orbit, and the central carbon constructs a one-membered orbit.

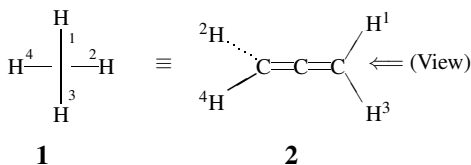


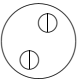
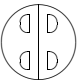
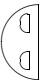
Figure 1: Convention for drawing allene derivatives

According to Fujita’s method [21], an orbit has its sphericity, so that the orbit is classified into a homospheric, enantiospheric, or hemispheric one, as cited in Table 1. The symbol \odot represents an achiral object of such an orbit as a result of the definition of the term “homospheric” shown in Table 1. The symbols \odot and \odot represent chiral objects in agreement with the definitions of the terms “enantiospheric” and “hemispheric” shown in Table 1. The large circles for the terms “homospheric” and “enantiospheric” represent achiral molecules, while the large semicircle for the term “hemispheric” represents a chiral molecule.

Objects accommodated in an orbit are governed by the sphericity of the orbit, where the mode of accommodation is called “chirality fittingness”, as collected in Table 2 [21]. The chirality/chirality of an object collected in Table 2 is determined in isolation. It should be noted that even an achiral object in isolation is restricted to be chiral if it is accommodated in an enantiospheric or hemispheric orbit.

In order to characterize the sphericity and the size of an orbit, a sphericity index is defined as a_d for a homospheric orbit, c_d for an enantiospheric orbit, and b_d for a hemispheric orbit,

Table 1: Sphericity of an orbit [21]

sphericity	orbit model	definition
homospheric		Among roto reflections that fix an orbit in an achiral molecule, there exists a roto reflection that fixes an object (Ⓢ) in the orbit.
enantiospheric		Among roto reflections that fix an orbit in an achiral molecule, there exists no roto reflection that fixes an object (Ⓢ or Ⓣ) in the orbit.*
hemispheric		There exist no roto reflections that fix an orbit in a chiral molecule.

*An object in an enantiospheric orbit may be achiral or chiral in isolation. Even an achiral object in isolation is restricted to be chiral in molecule when accommodated in the enantiospheric orbit.

where the subscript d represents the size of the orbit (Table 2).

Table 2: Sphericity Indices and Chirality Fittingness [21]

sphericity	sphericity index	chirality fittingness (allowed objects)*
homospheric	a_d	achiral objects
enantiospheric	c_d	achiral objects and chiral objects**
hemispheric	b_d	achiral objects and chiral objects

*The chirality/achirality is determined in isolation.

**Achiral objects in an enantiospheric orbit are divided into two halves. A d -membered enantiospheric orbit can accommodate $d/2$ of chiral objects and $d/2$ of their enantiomeric objects.

As discussed in the preceding paragraphs, the sphericity of an orbit and related matters are examined stepwise as follows [21]:

1. **Find equivalent objects** to construct an orbit.
2. **Test the sphericity of the orbit** according to the criteria listed in Table 1.
3. **Assign a sphericity index** according to the method listed in Table 2.
4. **Confirm the chirality fittingness** of each object according to Table 2.

Following this stepwise procedure, any objects in a molecule can be examined with respect to whether they are related symmetrically to each other.

2.2 Sphericities of Orbits in Allene Derivatives

Any objects can be selected as the members of an orbit so that orbits of various types appear concurrently, as shown in Table 3 for an allene molecule (**1**). Table 3 summarizes orbit sizes, sphericities, sphericity indices, and related properties of the orbits involved in **1**. For example, one ($H^{(1)}$) of the four hydrogens on the allene molecule (**1**) is immobile on the action of a reflection operator due to the mirror plane containing $H^{(1)}-C-H^{(3)}$. Hence, the corresponding 4-membered orbit is homospheric in the light of the criterion shown in Table 1, so that the sphericity index a_4 is assigned to the orbit.

On the other hand, any one of the four diagonal edges, i.e., $H^{(1)} \dots H^{(2)}$, $H^{(2)} \dots H^{(3)}$, $H^{(3)} \dots H^{(4)}$, and $H^{(4)} \dots H^{(1)}$, is not fixed by roto-reflections specified in the criteria listed in Table 1. Hence, the corresponding 4-membered orbit is concluded to be enantiospheric, so that the sphericity index c_4 is assigned to the orbit. In contrast, any one of the two horizontal edges, i.e., $H^{(1)} \dots H^{(3)}$ and $H^{(2)} \dots H^{(4)}$, is fixed by a roto-reflection (the mirror plane containing $H^{(1)}-C-H^{(3)}$). According to the criteria listed in Table 1, the corresponding 2-membered orbit is concluded to be homospheric, so that the sphericity index a_2 is assigned to the orbit.

The USCI-CF (unit-subduced-cycle-index with chirality fittingness) row of Table 3 lists a product of sphericity indices when two or more orbits of different or the same kinds are involved in the molecule; in the present case, each USCI-CF is equal to the sphericity index because there is a single orbit with respect to one kind of objects. The USCI (unit-subduced-cycle-index) row lists a product of sphericity indices without chirality fittingness, where the sphericity indices a_d , c_d , and b_d are replaced by a single dummy variable s_d .

Table 3: Orbits, sphericity indices, and coset representations in an allene molecule (**1**).

object type	vertex (bond)	diagonal edge	horizontal edge	terminal carbon	valence angle (plane)
objects in allene	H atoms (C–H bonds)	e.g., $H^{(1)} \dots H^{(2)}$	e.g., $H^{(1)} \dots H^{(3)}$	*C=C=C*	$\angle H-C-H$ ($\Delta H-C-H$)
orbit size	4	4	2	2	2
sphericity	homospheric	enantiospheric	homospheric	homospheric	homospheric
sphericity index (SI)	a_4	c_4	a_2	a_2	a_2
USCI-CF	a_4	c_4	a_2	a_2	a_2
USCI	s_4	s_4	s_2	s_2	s_2

2.3 Sphericity Indices During Desymmetrization

Let us consider the desymmetrization of the allene molecule **1** into a fluoroallene molecule (**3**), which belongs to C_s (Fig. 2). This desymmetrization concurrently influences the above-described objects in the allene molecule (Table 3), as shown in Table 4.

The fluorine atom in the fluoroallene molecule (**3**) constructs a one-membered orbit, which is homospheric because a reflection operation fixes the fluorine atom [21]. See the criterion listed in Table 1. The sphericity index a_1 is assigned to this orbit according to Table 2. The

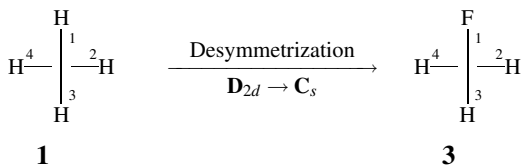


Figure 2: Desymmetrization of allene into fluoroallene

Table 4: Desymmetrization of orbits for a fluoroallene molecule (**3**)

object type	vertex (bond)	diagonal edge	horizontal edge	terminal carbon	valence angle (plane)
objects in allene	F atom (C–F bond)	e.g., F ⁽¹⁾ ...H ⁽²⁾	F ⁽¹⁾ ...H ⁽³⁾	C=C=C*	\angle F–C–H (Δ F–C–H)
orbit size	1	2	1	1	1
sphericity	homospheric	enantiospheric	homospheric	homospheric	homospheric
sphericity index (SI)	a_1	c_2	a_1	a_1	a_1
objects in allene	H atom (C–H bond)	e.g., H ⁽²⁾ ...H ⁽³⁾	H ⁽²⁾ ...H ⁽⁴⁾	*C=C=C	\angle H–C–H (Δ H–C–H)
orbit size	1	2	1	1	1
sphericity	homospheric	enantiospheric	homospheric	homospheric	homospheric
sphericity index (SI)	a_1	c_2	a_1	a_1	a_1
objects in allene	H atoms (C–H bonds)				
orbit size	2				
sphericity	enantiospheric				
sphericity index (SI)	c_2				
USCI-CF	$a_1^2 c_2$	c_2^2	a_1^2	a_1^2	a_1^2
USCI	$s_1^2 s_2$	s_2^2	s_1^2	s_1^2	s_1^2

three hydrogen atoms in the fluoroallene molecule (**3**) are divided into two orbits, i.e., a one-membered orbit (H⁽³⁾) and a two-membered orbit (H⁽²⁾ and H⁽⁴⁾). The former is homospheric so as to be characterized by a_1 in a similar way described for the orbit of the fluorine atom. The latter is enantiospheric, because no rotoreflection fixes anyone of the hydrogen atoms (Table 1). Hence, the orbit is characterized by a sphericity index c_2 , where the letter c indicates the enantiosphericity and the subscript 2 represents the size of the orbit (Table 2).

Because the fluoroallene molecule has two one-membered homospheric orbits (F or H, each a_1) and one two-membered enantiospheric orbit (H₂, c_2), the molecule can be characterized by the product of such sphericity indices as $a_1^2 c_2$. The product is called *unit subdued cycle*

index with chirality fittingness (USCI-CF). If sphericities are not taken into consideration, a unit subdivided cycle index without chirality fittingness (USCI) can be used, i.e., $s_1^2s_2$. The USCI-CFs collected in Tables 1 and 2 shows that the desymmetrization of allene (**1**) into fluoroallene (**3**) is characterized by the change of USCI-CFs, $a_4 \rightarrow a_1^2c_2$.

Exercise 1. Compare the symmetry of fluoroallene (**3**) with that of 1-chloro-1-fluoroallene (cf. **9** listed in Fig. 3).

On the same line, the objects of other types in the fluoroallene molecule are categorized into orbits, to which sphericity indices are assigned, as shown in Table 2. Thereby, the corresponding USCI-CFs and USCIs are calculated (the bottom of Table 2).

As a result, the desymmetrization of allene (**1**) into fluoroallene (**3**) shown in Fig. 2 causes concurrent desymmetrizations of the relevant orbits, which are characterized by comparing the USCI-CFs (or USCIs) collected in Tables 1 and 2. For example, the desymmetrization $a_4 \rightarrow a_1^2c_2$ for the four vertices as described above, the desymmetrization $a_4 \rightarrow c_2^2$ for the diagonal edges, the desymmetrization $a_2 \rightarrow a_1^2$ for the horizontal edges, etc. concur during the process shown in Fig. 2.

2.4 Allene Derivatives Produced by Desymmetrization

As found in the preceding subsection, the desymmetrization of allene (**1**) of D_{2d} -symmetry into fluoroallene (**3**) of C_s -symmetry (Fig. 2), which takes place as the result of the substitution of a fluorine atom, can be characterized by the change of USCIs for vertices ($s_4 \rightarrow s_1^2s_2$) as well as by the change of USCI-CFs for vertices ($a_4 \rightarrow a_1^2c_2$). In general, such changes of USCIs and of USCI-CFs can be used as probes for testing the existence or nonexistence of desymmetrized molecules, if they are combined with the group-subgroup relationship [25].

Following the method previously described by Fujita [25], the desymmetrization of allene (**1**) is depicted in Fig. 3 in the combination of the group-subgroup relationship of the point group D_{2d} , where we focus our attention on vertex desymmetrization. This type of diagrams is here called *subduction diagrams*. It should be noted that the USCIs and USCI-CFs used in the present method are obtained intuitively [21, 22], while those used in the original method [25] were obtained by a mathematical treatment.

Representative molecules for respective symmetries are depicted in Fig. 3, where two symmetries linked with a solid line represent a supergroup-subgroup relationship. A USCI listed below each molecule is marked by a symbol \bigcirc if the molecule can exist symmetrically and by a symbol \times if the molecule is impossible to exist symmetrically, where we consider the substitution of atoms or achiral ligands (H, X, Y, and Z) only. On the other hand, a mark at the top of each USCI-CF represents the existence (\bigcirc) or nonexistence (\times) of the corresponding molecule, where we consider the substitution of chiral ligands (p and \bar{p} as a pair of enantiomers) and achiral ligands or atoms.

It is worthwhile to examine the cases marked by the symbol \times in Fig. 3. For example, a D_2 -molecule is not realized within the substitution of atoms or achiral ligands, but can be realized to give **4** when chiral ligands (p) are permitted. This result is explained by the fact that the group D_2 has the same USCI (s_4) as the supergroup D_{2d} has, while the USCI-CF of the group D_2 (b_4) is different from that of the supergroup D_{2d} (a_4). The same situation holds true for an S_4 -molecule (**5**), where the USCI (s_4) is the same as that of **1**, while the USCI-CF (c_4) is different from that (a_4) of **1**.

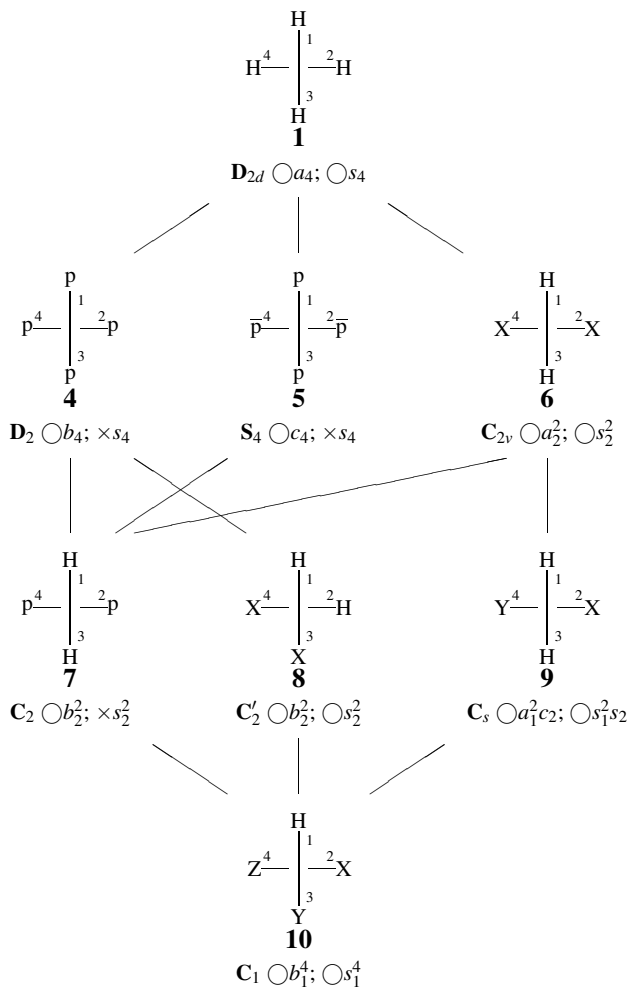


Figure 3: Subduction diagram with USCIs and USCI-CFs for testing the existence or nonexistence of allene derivatives during vertex substitution. The symbol \bigcirc shows the existence of a desymmetrized molecule, while the symbol \times shows the nonexistence of a desymmetrized molecule. Each USCI is concerned with the substitution of atoms or achiral (pro)ligands (H, X, Y, and Z) only, while each USCI-CF is concerned with the substitution of chiral (pro)ligands (p and \overline{p} as a pair of enantiomers) and achiral ones or atoms.

A C_2 -molecule (**7**) exhibits more complicated features because there exist three supergroups (D_2 , S_4 , and C_{2v}), as linked upward with solid lines (Fig. 3). Because the USCI (s_2^2) of C_2 is the same as that of **6** of C_{2v} , it is impossible to realize any C_2 -molecule within the substitution of atoms and achiral ligands. Because the USCI-CF (b_2^2) of C_2 is different from all the USCI-CFs of the supergroups (b_4 for D_2 , c_4 for C_{2v} , and a_2^2 for C_{2v}), such a molecule as **7** can be realized by considering chiral ligands (p).

Exercise 2. Construct a subduction diagram of oxirane derivatives (C_{2v}) by following the procedure described for Fig. 3. See Ref. [25].

Exercise 3. Construct a subduction diagram of cyclopropane derivatives (D_{3h}) by following the procedure described for Fig. 3. For the point group D_{3h} , see Ref. [26].

2.5 Molecules/Ligands vs. Promolecules/Proligands

For further discussion on stereochemistry and stereoisomerism, the term “ligand” should be used more rigorously than the conventional usage. In the conventional usage, for example, the letters a, b, c, and d of a tetrahedral molecule Cabcd or the letters a, b, ℓ^+ , and ℓ^- of a tetrahedral molecule $Cab\ell^+\ell^-$ have been used to designate atoms, achiral ligands, chiral ligands, or “point ligands” without rigorous definitions. In particular, the discrimination of “atoms, achiral and chiral ligands” from “point ligands” has not been well-defined so that nonrigid molecules having rotatable ligands have not been well treated within the conventional usage of the term.

Fujita has defined *proligands* as hypothetical ligands that have chirality/achirality only [27]. Then, he has defined a *promolecule* as a skeleton that accommodates such proligands in its substitution positions. Thereby, such a promolecule can be regarded as a rigid geometrical object. According to this formulation, a molecule, even though it is rigid or nonrigid, can be treated as an object in which the proligands of a promolecule are replaced by ligands.

Note that such a promolecule is regarded as a rigid object and that such ligands are regarded as rigid objects. Hence, the problem to be solved is to find requisites for converting a promolecule into a molecule. The concept of sphericity (Table 1) is shown to be a key concept during this procedure, because it is applicable both to molecules/ligands and to promolecules/proligands.

Strictly speaking, subduction diagrams (e.g., Fig. 3) discussed in the preceding section have implicitly based on the concept of proligand. It follows that the point-group symmetries collected in Fig. 3 are concerned with promolecules having proligands.

2.6 Deficient Subgroups

There appear allene derivatives corresponding to all of the subgroups of D_{2d} , when achiral and chiral ligands are taken into consideration, as shown in Fig. 3. However, this does not hold true even if we consider molecules of liganacy 4 [22]. In other words, there sometimes appears a case in which both the USCI and the USCI-CF for a group are equal to the USCI and the USCI-CF for either one of its supergroups. For example, D_{2d} - and D_2 -molecules (strictly speaking D_{2d} - and D_2 -promolecules [27]) are nonexistent among methane derivatives of T_d -symmetry, as shown in a subduction diagram (Fig. 4). Note that the term “ligands” is here used in the meaning of “proligands” (structureless objects with chirality/achirality). The nonexistence has been pointed out in a previous educational report [28] and explained in terms of the corresponding USCIs and USCI-CFs that have been algebraically calculated [25].

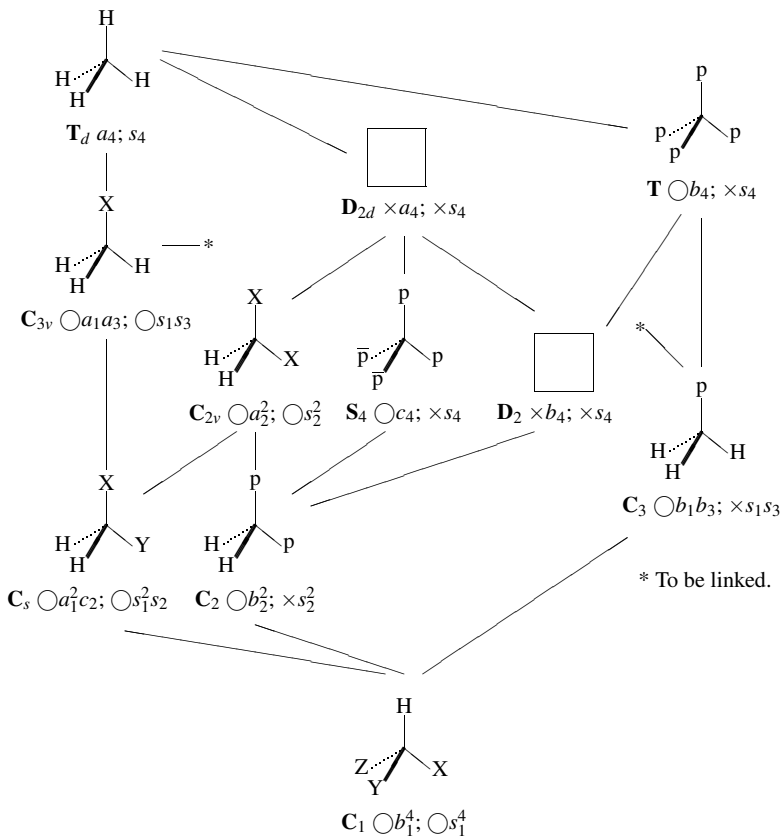


Figure 4: Subduction diagram with USCIs and USCIs-CFs for testing the existence or nonexistence of methane derivatives during vertex substitution [22]. For the symbols, see the caption of Fig. 3. The USCIs-CFs and USCIs for \mathbf{D}_{2d} and \mathbf{D}_2 are taken from Fig. 3 (see the text).

Exercise 4. Construct the subduction diagram (Fig. 4) by following the procedure described for Fig. 3. See Refs. [25, 22].

In the present paper, we take a non-mathematical approach in which USCIs and USCIs-CFs are obtained non-algebraically. This approach has some apparent difficulties. Because of the nonexistence of \mathbf{D}_{2d} - and \mathbf{D}_2 -derivatives of methane, one finds that the method described in the preceding subsections is not effective to obtain the USCIs and USCIs-CFs of the corresponding symmetries, so long as the methane skeleton only is taken into consideration. The vacancy of such USCIs and USCIs-CFs can be filled by additionally considering an allene skeleton, the results of which is shown in Fig. 3. Note that the central carbon atom of the methane skeleton is replaced conceptually by an allene axis ($\text{C}=\text{C}=\text{C}$) to give the allene skeleton.

As shown in Figs. 3 and 4, there are such compensated skeletons as allene and methane to fill vacant data of subgroups in the case of ligancy 4. However, this approach requires two or more skeletons, the selection of which is not so easy to be formulated. A more straightforward and general procedure using a *single skeleton* is desirable to systematize diagrammatical studies on molecular symmetry (cf. Section 4).

3 Global and Local Symmetries for Coset Representations

Before we pursue such a more straightforward and general procedure, we have to demonstrate the relationship between sphericity indices and coset representations. For this purpose, this section deals with an intuitive approach by starting global and local symmetries, although the relationship has been already examined mathematically in previous papers [11, 29] and Fujita's book [12]. The subjects of this section have introductorily been discussed in a previous educational article [24], where methane derivatives have been used as examples. For the sake of convenience for the present series of discussions, they are restated by using the allene derivatives described above.

3.1 Symmetry Operations as Elements of Groups

This section on the point group D_{2d} for an allene skeleton is based on Chapter 2 of Fujita's book [12]. An allene skeleton is superposable on itself on the action of symmetry operations shown in Fig. 5. The left diagram of Fig. 5 shows three two-fold rotations ($C_{2(1)}$, $C_{2(2)}$, and $C_{2(3)}$) around symmetry axes, which are perpendicular to one another as designated by vector symbols. The three two-fold rotations and an identity operation (I) are referred to as "proper rotations". The right diagram of Fig. 5 shows rotoreflections, which are two mirror reflections ($\sigma_{d(1)}$ and $\sigma_{d(2)}$) and four-fold rotation-reflections (S_4 and S_4^3).³ They are referred to as "improper rotations".

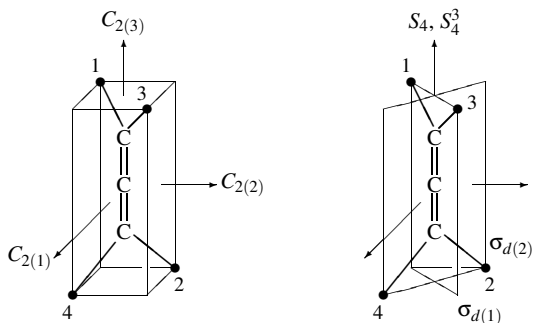


Figure 5: Symmetry operations of an allene molecule. Proper rotations are depicted in the left diagram, while improper rotations (rotoreflections) are depicted in the right diagram.

³The rotoreflection S_4 is a combined operation which consists of an anti-clockwise rotation by 90° and a horizontal reflection. The rotoreflection S_4^3 is a combined operation which consists of a clockwise rotation by 90° and a horizontal reflection.

The totally eight symmetry operations construct a group:

$$\mathbf{D}_{2d} = \{I, C_{2(3)}, C_{2(1)}, C_{2(2)}; \sigma_{d(1)}, \sigma_{d(2)}, S_4, S_4^3\}, \quad (1)$$

which is closed with respect to the multiplication of the operations. Among the subsets of the \mathbf{D}_{2d} , there are subsets which are closed by the same multiplication. They are called *subgroups*:

$$\mathbf{D}_2 = \{I, C_{2(3)}, C_{2(1)}, C_{2(2)}\} \quad (2)$$

$$\mathbf{C}_{2v} = \{I, C_{2(3)}; \sigma_{d(1)}, \sigma_{d(2)}\} \quad (3)$$

$$\mathbf{S}_4 = \{I, C_{2(3)}; S_4, S_4^3\} \quad (4)$$

$$\mathbf{C}_2 = \{I, C_{2(3)}\} \quad (5)$$

$$\mathbf{C}'_2 = \{I, C_{2(1)}\}, \quad \mathbf{C}''_2 = \{I, C_{2(2)}\} \quad (6)$$

$$\mathbf{C}_s = \{I, \sigma_{d(1)}\}, \quad \mathbf{C}'_s = \{I, \sigma_{d(2)}\} \quad (7)$$

$$\mathbf{C}_1 = \{I\}. \quad (8)$$

Among them, \mathbf{C}'_2 and \mathbf{C}''_2 are conjugate to each other, because the corresponding two-fold axes are superposable by an operator of \mathbf{D}_{2d} . This feature is designated by the equation: $S_4^{-1}C'_2S_4 = C''_2$. Similarly, \mathbf{C}_s and \mathbf{C}'_s are conjugate to each other because the corresponding mirror planes are superposable by an operator of \mathbf{D}_{2d} . This feature is designated by the equation: $S_4^{-1}C_sS_4 = C'_s$.

By regarding conjugate subgroups as being equivalent, a non-redundant set of subgroups (SSG) is selected as follows:

$$\text{SSG}_{\mathbf{D}_{2d}} = \{\mathbf{C}_1, \mathbf{C}_2, \mathbf{C}'_2, \mathbf{C}_s, \mathbf{S}_4, \mathbf{C}_{2v}, \mathbf{D}, \mathbf{D}_{2d}\}, \quad (9)$$

which are aligned in an ascending order of their orders ($|\mathbf{C}_1| = 1$, $|\mathbf{C}_2| = 2$, $|\mathbf{C}'_2| = 2$, $|\mathbf{C}_s| = 2$, $|\mathbf{S}_4| = 4$, $|\mathbf{C}_{2v}| = 4$, $|\mathbf{D}| = 4$, and $|\mathbf{D}_{2d}| = 8$). Obviously, Fig. 3 is implicitly based on the SSG (eq. 9).

The subgroups of \mathbf{D}_{2d} are categorized into two types: chiral subgroups (\mathbf{D} , \mathbf{C}_2 , \mathbf{C}'_2 , \mathbf{C}''_2), and \mathbf{C}_1) that consist of proper rotations only and achiral subgroup (\mathbf{D}_{2d} , \mathbf{C}_{2v} , \mathbf{S}_4 , \mathbf{C}_s , \mathbf{C}'_2) that consist of proper and improper rotations.

3.2 Orbits and Coset Representations

Table 1 can be sophisticated by using a local symmetry (a subgroup) in place of three types of fixing operations described in the definition column. Let \mathbf{G} be the symmetry of a molecule having an orbit of objects, where the group \mathbf{G} is called the *global symmetry*. In addition to a rotoreflection used in the definitions of Table 1, there are a set of operations that fixes (stabilizes) an object at issue. The set of operations constructs a group (\mathbf{H}), which is called the *local symmetry* of the orbit. Mathematically (group-theoretically) speaking, the local symmetry \mathbf{H} is referred to as a *stabilizer*.

The global symmetry \mathbf{G} and the local symmetry \mathbf{H} are combined by a coset decomposition, which produces a permutation representation called a *coset representation* (CR). The symbol $\mathbf{G}/(\mathbf{H})$ has been coined to designate such a CR for the sake of simplicity [11, 12]. As a result, we can say that the orbit is governed by the CR $\mathbf{G}/(\mathbf{H})$. The correspondence between the orbit and the CR $\mathbf{G}/(\mathbf{H})$ allows us to refer to the orbit as a $\mathbf{G}/(\mathbf{H})$ -orbit.

As discussed in the preceding paragraphs, a CR can be obtained stepwise as follows:

Table 5: Coset Representation (\mathbf{G}/\mathbf{H}) and Sphericity Indices [11]

global symmetry (\mathbf{G})	local symmetry (\mathbf{H})	sphericity	sphericity index (where $d = \mathbf{G} / \mathbf{H} $)
achiral	achiral	homospheric	a_d
achiral	chiral	enantiospheric	c_d
chiral	chiral	hemispheric	b_d

1. **Find the global symmetry \mathbf{G}** of a molecule.
2. **Find equivalent objects** to construct an orbit.
3. **Find the local symmetry \mathbf{H}** of the orbit.
4. **Assign the corresponding CR \mathbf{G}/\mathbf{H}** by combining the global symmetry and the local symmetry.

Following this stepwise procedure, any objects in a molecule can be examined with respect to whether they are related symmetrically to each other. It should be emphasized that the present approach uses the symbol \mathbf{G}/\mathbf{H} without calculating the concrete form, whereas the original USCI approach calculated the concrete form of the CR [11, 12].

The sphericity of the orbit is defined alternatively by examining whether the global symmetry \mathbf{G} and the local symmetry \mathbf{H} are achiral or chiral, as shown in Table 5. The degree (length) of the CR is calculated to be $|\mathbf{G}|/|\mathbf{H}|$, which is equal to the size of the orbit, i.e., $d = |\mathbf{G}|/|\mathbf{H}|$. Thereby, the corresponding sphericity index is alternatively obtained: a_d , c_d , or b_d , where we place $d = |\mathbf{G}|/|\mathbf{H}|$ (Table 5).

The comparison between Table 2 and Table 5 indicates the close relationship between the sphericity index and the CR. Thus, the sphericity index put a special emphasis on the chirality/achirality of each object in an orbit, while the CR is concerned with the local symmetry of each object in an orbit. Because the orbit is controlled by the corresponding global symmetry, the sphericity and the CR are capable of treating *inner structures* in a molecule.

Table 6 shows such local symmetries for the orbits collected in Table 3. For example, the hydrogen at the vertex 1 (Fig. 5) is fixed by the operations of \mathbf{C}_s ($= \{I, \sigma_{d(1)}\}$) so that the corresponding orbit (the four hydrogens) is assigned to the local symmetry of \mathbf{C}_s . The local symmetry \mathbf{C}_s and the global symmetry \mathbf{D}_{2d} are combined by a coset decomposition, which produces the CR $\mathbf{D}_{2d}/\mathbf{C}_s$. Because both \mathbf{D}_{2d} and \mathbf{C}_s are achiral, the sphericity of the orbit is determined to be homospheric. The degree of the CR $\mathbf{D}_{2d}/\mathbf{C}_s$ is calculated to be $|\mathbf{D}_{2d}|/|\mathbf{C}_s| = 8/2 = 4$, where $|\mathbf{D}_{2d}| (= 8)$ and $|\mathbf{C}_s| (= 2)$ represent the orders of the respective groups. Hence, the sphericity index is calculated to be a_4 , which is identical with the one collected in Table 3.

On the same line, the other objects shown in Table 3 are correlated to the corresponding CRs, as collected in Table 6.

3.3 Desymmetrization of Orbits and Subduction of Coset Representations

The derivation of fluoroallene (**3**) from **1** is accompanied by the desymmetrization from \mathbf{D}_{2d} to \mathbf{C}_s , as shown in Fig. 2. The one-membered orbit of $\mathbf{H}^{(3)}$ (or $\mathbf{F}^{(1)}$) has a local symmetry

Table 6: Orbits and coset representations in an allene molecule (**1**).

object type	vertex (bond)	diagonal edge	horizontal edge	terminal carbon	valence angle (plane)
objects in allene	H atoms (C–H bonds)	e.g., $H^{(1)} \dots H^{(2)}$	e.g., $H^{(1)} \dots H^{(3)}$	*C=C=C*	$\angle H-C-H$ ($\triangle H-C-H$)
local symmetry	C_s	C_2'	C_{2v}	C_{2v}	C_{2v}
CR	D_{2d}/C_s	D_{2d}/C_2'	D_{2d}/C_{2v}	D_{2d}/C_{2v}	D_{2d}/C_{2v}
degree of CR	$ D_{2d} / C_s $ = $8/2 = 4$	$ D_{2d} / C_2' $ = $8/2 = 4$	$ D_{2d} / C_{2v} $ = $8/4 = 2$	$ D_{2d} / C_{2v} $ = $8/4 = 2$	$ D_{2d} / C_{2v} $ = $8/4 = 2$
sphericity	homospheric	enantiospheric	homospheric	homospheric	homospheric
sphericity index (SI)	a_4	c_4	a_2	a_2	a_2
USCI-CF	a_4	c_4	a_2	a_2	a_2
USCI	s_4	s_4	s_2	s_2	s_2

C_s so that it is assigned to the CR $C_s(/C_s)$. The two-membered orbit of $\{H^{(2)}, H^{(4)}\}$ has a local symmetry C_1 so that it is assigned to the CR $C_s(/C_1)$. This means that the original orbit D_{2d}/C_s is desymmetrized into C_s so as to be divided into two homospheric $C_s(/C_s)$ -orbits and one enantiospheric $C_s(/C_1)$ -orbit. This is represented by the following equation:

$$D_{2d}/C_s \downarrow C_s = 2C_s(/C_s) + C_s(/C_1), \quad (10)$$

which is called the subduction of a coset representation. This is listed in the vertex column of Table 7. The result listed in the right-hand side of eq. 10 corresponds to the USCI-CF ($a_1^2 c_2$) listed in Table 4.

It should be noted that the orbit size calculated by $|D_{2d}|/|C_s|$ ($= 8/2 = 4$) based on the left-hand side of eq. 10 is equal to the sum calculated by $2|C_s|/|C_s| + |C_s|/|C_1|$ ($= 2 \times (2/2) + 2/1 = 4$) based on the right-hand side. Thus the number of objects is conserved, although this result is obvious.

Similarly, the other orbits can be characterized by the subductions of CRs:

$$D_{2d}/C_2' \downarrow C_s = 2C_s(/C_1) \quad (11)$$

$$D_{2d}/C_{2v} \downarrow C_s = 2C_s(/C_s), \quad (12)$$

which are derived from the data of Table 7. The conservation of the number of objects is also confirmed by eqs. 11 and 12. In fact, $|D_{2d}|/|C_2'|$ ($= 8/2 = 4$) based on the left-hand side of eq. 11 is equal to the sum calculated by $2|C_s|/|C_1|$ ($= 2 \times (2/1) = 4$) based on the right-hand side. Further, $|D_{2d}|/|C_{2v}|$ ($= 8/4 = 2$) based on the left-hand side of eq. 12 is equal to the sum calculated by $2|C_s|/|C_s|$ ($= 2 \times (2/2) = 2$) based on the right-hand side.

Whereas subductions of CRs such as eqs. 10–12 can be algebraically calculated for representative point groups and collected in Appendix of Fujita's book [12], the present diagrammatical approach is effective to chemical applications because of its convenience. However, such vacant data of subgroups as depicted in Fig. 4 still remain as troublesome cases even in the diagrammatical approach for obtaining subductions of CRs. It follows that a more straightforward

Table 7: Desymmetrization of orbitals for a fluoroallene molecule

object type	vertex (bond)	diagonal edge	horizontal edge	terminal carbon	valence angle (plane)
objects	F atom	e.g.,		C=C=C*	$\angle\text{F}-\text{C}-\text{H}$
in allene	(C-F bond)	$\text{F}^{(1)} \dots \text{H}^{(2)}$	$\text{F}^{(1)} \dots \text{H}^{(3)}$		$(\Delta\text{F}-\text{C}-\text{H})$
local symmetry	C_s	C_1	C_s	C_s	C_s
CR	$\text{C}_s(/ \text{C}_s)$	$\text{C}_s(/ \text{C}_1)$	$\text{C}_s(/ \text{C}_s)$	$\text{C}_s(/ \text{C}_s)$	$\text{C}_s(/ \text{C}_s)$
degree	$ \text{C}_s / \text{C}_s $	$ \text{C}_s / \text{C}_1 $	$ \text{C}_s / \text{C}_s $	$ \text{C}_s / \text{C}_s $	$ \text{C}_s / \text{C}_s $
of CR	$= 2/2 = 1$	$= 2/1 = 2$	$= 2/2 = 1$	$= 2/2 = 1$	$= 2/2 = 1$
sphericity	homospheric	enantiospheric	homospheric	homospheric	homospheric
sphericity index (SI)	a_1	c_2	a_1	a_1	a_1
objects	H atom	e.g.,		*C=C=C	$\angle\text{H}-\text{C}-\text{H}$
in allene	(C-H bond)	$\text{H}^{(2)} \dots \text{H}^{(3)}$	$\text{H}^{(2)} \dots \text{H}^{(4)}$		$(\Delta\text{H}-\text{C}-\text{H})$
local symmetry	C_s	C_1	C_s	C_s	C_s
CR	$\text{C}_s(/ \text{C}_s)$	$\text{C}_s(/ \text{C}_1)$	$\text{C}_s(/ \text{C}_s)$	$\text{C}_s(/ \text{C}_s)$	$\text{C}_s(/ \text{C}_s)$
degree	$ \text{C}_s / \text{C}_s $	$ \text{C}_s / \text{C}_1 $	$ \text{C}_s / \text{C}_s $	$ \text{C}_s / \text{C}_s $	$ \text{C}_s / \text{C}_s $
of CR	$= 2/2 = 1$	$= 2/1 = 2$	$= 2/2 = 1$	$= 2/2 = 1$	$= 2/2 = 1$
sphericity	homospheric	enantiospheric	homospheric	homospheric	homospheric
sphericity index (SI)	a_1	c_2	a_1	a_1	a_1
objects	H atoms				
in allene	(C-H bonds)				
local symmetry	C_1				
CR	$\text{C}_s(/ \text{C}_1)$				
degree	$ \text{C}_s / \text{C}_1 $				
of CR	$= 2/1 = 2$				
sphericity	enantiospheric				
sphericity index (SI)	c_2				
Subduction of CR	$2\text{C}_s(/ \text{C}_s) + \text{C}_s(/ \text{C}_1)$	$2\text{C}_s(/ \text{C}_1)$	$2\text{C}_s(/ \text{C}_s)$	$2\text{C}_s(/ \text{C}_s)$	$2\text{C}_s(/ \text{C}_s)$
USCI-CF	$a_1^2 c_2$	c_2^2	a_1^2	a_1^2	a_1^2
USCI	$s_1^2 s_2$	s_2^2	s_1^2	s_1^2	s_1^2

and general procedure using a single skeleton is again desirable to systematize diagrammatical studies on molecular symmetry. This is the target of the following sections.

4 Exhaustive Diagrammatical Derivation of Coset Representations

Whether sphericity indices (cf. Section 2) or subduction of CRs (cf. Section 3) are pursued as targets, a general procedure should be developed on the basis of a single skeleton, as pointed out in the last parts of Sections 2 and 3. This section deals with such a general procedure.

4.1 Regular Bodies

The concept of *regular body* has been proposed in a previous paper [30] and described in a general and mathematical fashion in Chapter 7 of Fujita's book [12]. A regular body of \mathbf{G} -symmetry is defined as a skeleton having a \mathbf{G}/\mathbf{C}_1 -orbit, where \mathbf{C}_1 represents an identity group, i.e., $\mathbf{C}_1 = \{I\}$. The corresponding CR \mathbf{G}/\mathbf{C}_1 is called a *regular representation*, where the degree of the CR is equal to $|\mathbf{G}|/|\mathbf{C}_1| = |\mathbf{G}|$.

In contrast to the previous approach for regular bodies [30, 12], the present approach adopts an intuitive definition of a regular representation, which is regarded as one extreme of CRs described above. Thus, we select an allene skeleton (**11**) as a regular body for \mathbf{D}_{2d} -symmetry (Fig. 6), where two cyclopropane units are linked with an allene axis (C=C=C) so as to be perpendicular to each other. Because this modification does not influence the symmetry of an allene skeleton, the regular body (**11**) also belongs to \mathbf{D}_{2d} , which is determined to be the global symmetry of the regular body as a skeleton. Each of the eight positions (vertices) of **11** is fixed only on the action of \mathbf{C}_1 , which is determined to be the local symmetry.⁴ Hence, the orbit of the eight positions (vertices) is concluded to be governed by the regular representation $\mathbf{D}_{2d}/\mathbf{C}_1$. The degree of the regular representation is calculated to be $|\mathbf{D}_{2d}|/|\mathbf{C}_1| = 8/1 = 8$, which is equal to the size of the orbit.

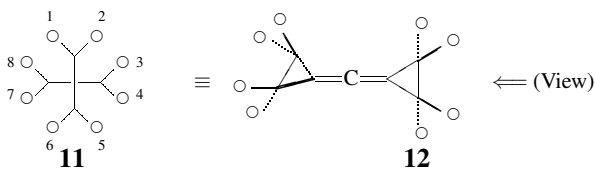


Figure 6: Regular body for \mathbf{D}_{2d} .

The vertices (or objects on the vertices) of the regular body (**11**) shown in Fig. 6 are numbered sequentially and the resulting orbit of vertices ($\mathcal{R} = \{1, 2, 3, 4, 5, 6, 7, 8\}$) is regarded as an ordered set. Then the vertices of \mathcal{R} generate permutations on the action of operations of \mathbf{D}_{2d} (eq.

⁴The vertices of the regular body (**11**) are regarded as substitution positions when **11** is considered to be a skeleton. The vertices are governed by the same CR \mathbf{G}/\mathbf{C}_1 as the objects (\circ , \bullet , etc.) accommodated by them. In particular, the vertices are sometimes equalized to hydrogen atoms on the vertices, because organic chemistry (especially organic nomenclature) considers the replacement of hydrogens by other atoms. This shift of viewpoints is permissible since it provides no confusion.

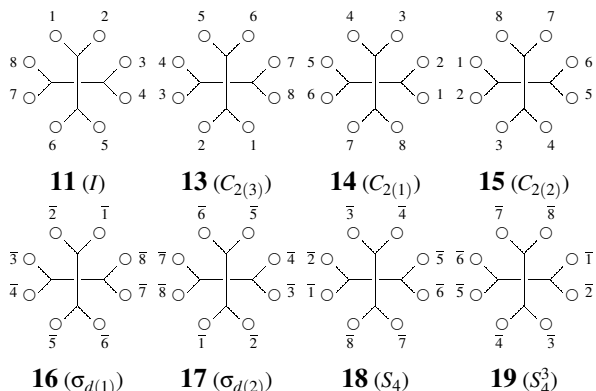


Figure 7: Permutation Diagram containing transformulas produced by symmetry operations onto a regular body for D_{2d} . The set of eight positions $\mathcal{R} = \{1, 2, 3, 4, 5, 6, 7, 8\}$ constructs an orbit governed by the regular representation $D_{2d}/(C_1)$ in terms of intramolecular stereochemistry.

1), as shown in Fig. 7. Such diagrams as Fig. 7 are here called *permutation diagrams*. For example, the action of $C_{2(3)}$ on the \mathcal{R} produces another ordered set, i.e., $\mathcal{R}_{C_{2(3)}} = \{5, 6, 7, 8, 1, 2, 3, 4\}$, as shown in **13**. This conversion (**11** into **13**) is represented by the following permutation:

$$\begin{pmatrix} 1 & 2 & 3 & 4 & 5 & 6 & 7 & 8 \\ 5 & 6 & 7 & 8 & 1 & 2 & 3 & 4 \end{pmatrix} = (1\ 5)(2\ 6)(3\ 7)(4\ 8), \quad (13)$$

where the right-hand side is represented as a product of cycles. Such formulas as generated by the action of symmetry operations (e.g., **11** by I and **13** by $C_{2(3)}$) are called here *transformulas*.⁵ Thus, the transformation of **11** into every one of the transformulas listed in Fig. 7 generates the following permutations (as products of cycles) for the respective operations:

$$I \sim \begin{pmatrix} 1 & 2 & 3 & 4 & 5 & 6 & 7 & 8 \\ 1 & 2 & 3 & 4 & 5 & 6 & 7 & 8 \end{pmatrix} = (1)(2)(3)(4)(5)(6)(7)(8) \quad (14)$$

$$C_{2(3)} \sim \begin{pmatrix} 1 & 2 & 3 & 4 & 5 & 6 & 7 & 8 \\ 5 & 6 & 7 & 8 & 1 & 2 & 3 & 4 \end{pmatrix} = (1\ 5)(2\ 6)(3\ 7)(4\ 8) \quad (15)$$

$$C_{2(1)} \sim \begin{pmatrix} 1 & 2 & 3 & 4 & 5 & 6 & 7 & 8 \\ 4 & 3 & 2 & 1 & 8 & 7 & 6 & 5 \end{pmatrix} = (1\ 4)(2\ 3)(5\ 8)(6\ 7) \quad (16)$$

$$C_{2(2)} \sim \begin{pmatrix} 1 & 2 & 3 & 4 & 5 & 6 & 7 & 8 \\ 8 & 7 & 6 & 5 & 4 & 3 & 2 & 1 \end{pmatrix} = (1\ 8)(2\ 7)(3\ 6)(4\ 5) \quad (17)$$

$$\sigma_{d(1)} \sim \begin{pmatrix} 1 & 2 & 3 & 4 & 5 & 6 & 7 & 8 \\ \bar{2} & \bar{1} & \bar{8} & \bar{7} & \bar{6} & \bar{5} & \bar{4} & \bar{3} \end{pmatrix} = \overline{(1\ 2)(3\ 8)(4\ 7)(5\ 6)} \quad (18)$$

⁵To denote such formulas generated by permutations, the term “configurations” has been used in Pólya’s book [8] and in Fujita’s book [12] while the term “homomer sets” has been used in a recent paper [31]. Because the terms “configuration” and “homomer” have been used in different meanings in chemistry, the term “transformulas” is coined tentatively in this article.

$$\sigma_{d(2)} \sim \left(\overline{\frac{1}{6}} \ \overline{\frac{2}{5}} \ \overline{\frac{3}{4}} \ \overline{\frac{4}{3}} \ \overline{\frac{5}{2}} \ \overline{\frac{6}{1}} \ \overline{\frac{7}{8}} \ \overline{\frac{8}{7}} \right) = \overline{(1\ 6)(2\ 5)(3\ 4)(7\ 8)} \quad (19)$$

$$S_4 \sim \left(\overline{\frac{1}{3}} \ \overline{\frac{2}{4}} \ \overline{\frac{3}{5}} \ \overline{\frac{4}{6}} \ \overline{\frac{5}{7}} \ \overline{\frac{6}{8}} \ \overline{\frac{7}{1}} \ \overline{\frac{8}{2}} \right) = \overline{(1\ 3\ 5\ 7)(2\ 4\ 6\ 8)} \quad (20)$$

$$S_4^3 \sim \left(\overline{\frac{1}{7}} \ \overline{\frac{2}{8}} \ \overline{\frac{3}{1}} \ \overline{\frac{4}{2}} \ \overline{\frac{5}{3}} \ \overline{\frac{6}{4}} \ \overline{\frac{7}{5}} \ \overline{\frac{8}{6}} \right) = \overline{(1\ 7\ 5\ 3)(2\ 8\ 6\ 4)} \quad (21)$$

where each overbar represents the mirror image of each object.⁶ The set of the permutations (eqs. 14—21) is a permutation representation based on the regular body (**11**) shown in Fig. 6. This permutation representation is characterized by the symbol $\mathbf{D}_{2d}/\langle C_1 \rangle$ because the local symmetry is determined to be C_1 . As discussed generally in Chapter 7 of Fujita's book [12], the permutation representation obtained diagrammatically by using the regular body (**11**) can be equalized to the corresponding CR which has been algebraically obtained by using a coset decomposition of \mathbf{D}_{2d} by C_1 . The CR $\mathbf{D}_{2d}/\langle C_1 \rangle$ as one extreme case is called a *regular representation*. It should be noted that the regular representation can be regarded as a multiplication table of \mathbf{D}_{2d} itself.

Because \mathbf{D}_{2d} is achiral and C_1 is chiral, a $\mathbf{D}_{2d}/\langle C_1 \rangle$ -orbit is enantiospheric according to the criterion of Table 5. This CR corresponds to a sphericity index c_8 because of $|\mathbf{D}_{2d}|/|C_1| = 8/1 = 8$.

4.2 Segments in Regular Bodies

Any set of objects in a molecule can be further regarded as a secondary object. As a result, the set of objects and its equivalent sets of objects can construct an orbit of another kind. The latter orbit has been formulated by the mathematical concept "blocks in a regular body" described in Ref. [30] and in Chapter 7 of Fujita's book [12]. This concept is here discussed more intuitively by using the term *segment* in a regular body. Whereas the term "blocks" designates any sets of objects, the term *segments* is used to designate sets of objects, if any two of such sets can be so selected as to have no common objects. If such segments have a chemical meaning, they are called *ligands*, as discussed in the next subsection.

4.2.1 Orbits of Segments Governed by the CR $\mathbf{D}_{2d}/\langle C_s \rangle$

For example, let us consider a set of two vertices, e.g., $\mathcal{A}_1 = \{1, 2\}$, which is regarded as a segment, as shown in **20** of Fig. 8. On the action of operations of \mathbf{D}_{2d} (eq. 1), the set \mathcal{A}_1 is converted into other segments, i.e., $\mathcal{A}_2 = \{3, 4\}$, $\mathcal{A}_3 = \{5, 6\}$, and $\mathcal{A}_4 = \{7, 8\}$. This means that the segments $\mathcal{A}_1, \mathcal{A}_2, \mathcal{A}_3$, and \mathcal{A}_4 are equivalent on the action of \mathbf{D}_{2d} so that the set of the segments $\mathcal{A} = \{\mathcal{A}_1, \mathcal{A}_2, \mathcal{A}_3, \mathcal{A}_4\}$ is over again regarded as an orbit. Because the segment \mathcal{A}_1 is fixed (stabilized) on the action C_s (eq. 7), the local symmetry of the orbit \mathcal{A} is determined to be C_s . Hence, the orbit \mathcal{A} is concluded to be governed by the CR $\mathbf{D}_{2d}/\langle C_s \rangle$. It should be noted that the segments \mathcal{A}_1 and \mathcal{A}_3 are fixed on the action C_s (eq. 7), while the segments \mathcal{A}_2 and \mathcal{A}_4 are fixed on the action C'_s (eq. 7). Because C_s and C'_s are conjugate within \mathbf{D}_{2d} , they are regarded as being equivalent in this treatment. Each segment of \mathcal{A} is called a C_s -segment because it is fixed (stabilized) on the action of C_s (or its conjugate subgroup C'_s).

⁶The conventional treatments based on permutation representations have not taken account of the mirror images of objects. This means that the inner structures of objects have been disregarded. In contrast, the present approach considers the inner structures of objects in the form of sphericities. The overbar shows this approach explicitly.

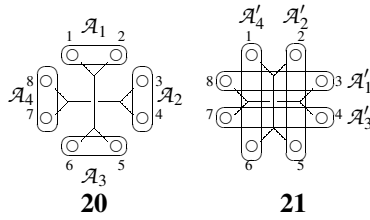


Figure 8: Segmentation patterns to generate orbits of C_s -segments in the regular body (11) for illustrating the CR $D_{2d}(/C_s)$. Each segment encircled by an oval is called a C_s -segment because it is fixed (stabilized) on the action of C_s (or its conjugate subgroup C'_s).

As shown in the right segmentation pattern (21) of Fig. 8, another orbit of segments governed by the CR $D_{2d}(/C_s)$ can be considered, i.e., $\mathcal{A}' = \{\mathcal{A}'_1, \mathcal{A}'_2, \mathcal{A}'_3, \mathcal{A}'_4\}$, where we place $\mathcal{A}'_1 = \{3, 8\}$, and $\mathcal{A}'_2 = \{2, 5\}$, $\mathcal{A}'_3 = \{4, 7\}$, $\mathcal{A}'_4 = \{1, 6\}$. Note that the segments \mathcal{A}'_1 and \mathcal{A}'_3 are fixed on the action of C_s (eq. 7), while the segments \mathcal{A}'_2 and \mathcal{A}'_4 are fixed on the action of C'_s (eq. 7), where C_s and C'_s are conjugate within D_{2d} .

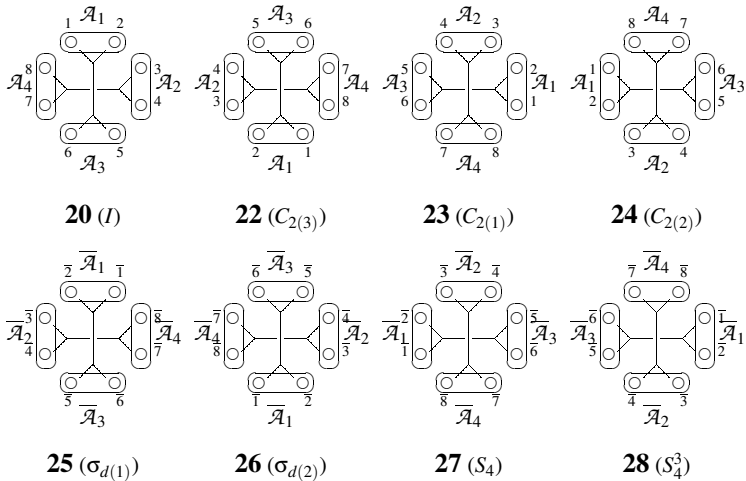


Figure 9: Permutation diagram containing transformulas generated on the action of the symmetry operations of D_{2d} on the set of segments $\mathcal{A} = \{\mathcal{A}_1, \mathcal{A}_2, \mathcal{A}_3, \mathcal{A}_4\}$ in a regular body. The set \mathcal{A} is an orbit governed by the CR $D_{2d}(/C_s)$. This diagram is regarded as being generated by the superposition of the segmentation pattern (20) onto Fig. 7.

Suppose that the orbit $\mathcal{A} = \{\mathcal{A}_1, \mathcal{A}_2, \mathcal{A}_3, \mathcal{A}_4\}$ shown in 20 of Fig. 8 is an ordered set. Then the segments involved in \mathcal{A} generate permutations on the action of operations of D_{2d} (eq. 1), as shown in Fig. 9. For example, the action of $C_{2(3)}$ on the \mathcal{A} produces another ordered set, i.e., $\{\mathcal{A}_3, \mathcal{A}_4, \mathcal{A}_1, \mathcal{A}_2\}$, as shown in 22. This process (20 into 22) is expressed by the permutation of

an ordered set $\{1, 2, 3, 4\}$ into another set $\{3, 4, 1, 2\}$ as follows:

$$\begin{pmatrix} \mathcal{A}_1 & \mathcal{A}_2 & \mathcal{A}_3 & \mathcal{A}_4 \\ \mathcal{A}_3 & \mathcal{A}_4 & \mathcal{A}_1 & \mathcal{A}_2 \end{pmatrix} = \begin{pmatrix} 1 & 2 & 3 & 4 \\ 3 & 4 & 1 & 2 \end{pmatrix} = (1\ 3)(2\ 4), \quad (22)$$

where the last expression is based on a product of cycles. Thereby, we can obtain the following permutations (as products of cycles) for the respective operations:

$$I \sim \begin{pmatrix} \mathcal{A}_1 & \mathcal{A}_2 & \mathcal{A}_3 & \mathcal{A}_4 \\ \mathcal{A}_1 & \mathcal{A}_2 & \mathcal{A}_3 & \mathcal{A}_4 \end{pmatrix} = (1)(2)(3)(4) \quad (23)$$

$$C_{2(3)} \sim \begin{pmatrix} \mathcal{A}_1 & \mathcal{A}_2 & \mathcal{A}_3 & \mathcal{A}_4 \\ \mathcal{A}_3 & \mathcal{A}_4 & \mathcal{A}_1 & \mathcal{A}_2 \end{pmatrix} = (1\ 3)(2\ 4) \quad (24)$$

$$C_{2(1)} \sim \begin{pmatrix} \mathcal{A}_1 & \mathcal{A}_2 & \mathcal{A}_3 & \mathcal{A}_4 \\ \mathcal{A}_2 & \mathcal{A}_1 & \mathcal{A}_4 & \mathcal{A}_3 \end{pmatrix} = (1\ 2)(3\ 4) \quad (25)$$

$$C_{2(2)} \sim \begin{pmatrix} \mathcal{A}_1 & \mathcal{A}_2 & \mathcal{A}_3 & \mathcal{A}_4 \\ \mathcal{A}_4 & \mathcal{A}_3 & \mathcal{A}_2 & \mathcal{A}_1 \end{pmatrix} = (1\ 4)(2\ 3) \quad (26)$$

$$\sigma_{d(1)} \sim \begin{pmatrix} \mathcal{A}_1 & \mathcal{A}_2 & \mathcal{A}_3 & \mathcal{A}_4 \\ \overline{\mathcal{A}_1} & \overline{\mathcal{A}_4} & \overline{\mathcal{A}_3} & \overline{\mathcal{A}_2} \end{pmatrix} = \overline{(1)(2\ 4)(3)} \quad (27)$$

$$\sigma_{d(2)} \sim \begin{pmatrix} \mathcal{A}_1 & \mathcal{A}_2 & \mathcal{A}_3 & \mathcal{A}_4 \\ \overline{\mathcal{A}_3} & \overline{\mathcal{A}_2} & \overline{\mathcal{A}_1} & \overline{\mathcal{A}_4} \end{pmatrix} = \overline{(1\ 3)(2)(4)} \quad (28)$$

$$S_4 \sim \begin{pmatrix} \mathcal{A}_1 & \mathcal{A}_2 & \mathcal{A}_3 & \mathcal{A}_4 \\ \overline{\mathcal{A}_2} & \overline{\mathcal{A}_3} & \overline{\mathcal{A}_4} & \overline{\mathcal{A}_1} \end{pmatrix} = \overline{(1\ 2\ 3\ 4)} \quad (29)$$

$$S_4^3 \sim \begin{pmatrix} \mathcal{A}_1 & \mathcal{A}_2 & \mathcal{A}_3 & \mathcal{A}_4 \\ \overline{\mathcal{A}_4} & \overline{\mathcal{A}_1} & \overline{\mathcal{A}_2} & \overline{\mathcal{A}_3} \end{pmatrix} = \overline{(1\ 4\ 3\ 2)}, \quad (30)$$

where each of the products of cycles in the right-hand sides is represented by the subscripts only and where each overbar represents the mirror image of each segment. The set of the permutations (eqs. 23—30) is a concrete form of the CR $\mathbf{D}_{2d}/(\mathbf{C}_s)$. As discussed generally in Chapter 7 of Fujita's book [12], the CR obtained diagrammatically by using the \mathbf{C}_s -segments (20) is equivalent to the corresponding CR which has been algebraically obtained by using a coset decomposition of \mathbf{D}_{2d} by \mathbf{C}_s .

Because both \mathbf{D}_{2d} and \mathbf{C}_s are achiral, a $\mathbf{D}_{2d}/(\mathbf{C}_s)$ -orbit is homospheric according to the criterion of Table 5. This CR corresponds to a sphericity index a_4 because of $|\mathbf{D}_{2d}|/|\mathbf{C}_s| = 8/2 = 4$. It should be noted that each segment of \mathcal{A} has an inner structure so that the permutations shown in Fig. 9 (for the CR $\mathbf{D}_{2d}/(\mathbf{C}_s)$) occur concurrently with the permutations shown in Fig. 7 (for the CR $\mathbf{D}_{2d}/(\mathbf{C}_1)$).

Exercise 5. Construct a permutation diagram for the orbit \mathcal{A}' by using the segmentation pattern **21** (Fig. 8). Then, show permutations corresponding to the orbit \mathcal{A}' . Compare these permutations with eqs. 23–30.

4.2.2 Orbits of Segments Governed by the CR $\mathbf{D}_{2d}/(\mathbf{C}'_2)$

Let us next consider four sets of two vertices, $\mathcal{B}_1 = \{2, 3\}$, $\mathcal{B}_2 = \{4, 5\}$, $\mathcal{B}_3 = \{6, 7\}$, and $\mathcal{B}_4 = \{1, 8\}$, which are regarded as segments, as shown in **29** of Fig. 10. They are equivalent on the action of operations of \mathbf{D}_{2d} (eq. 1) so as to construct an orbit, i.e., $\mathcal{B} = \{\mathcal{B}_1, \mathcal{B}_2, \mathcal{B}_3, \mathcal{B}_4\}$.

Because the segment \mathcal{B}_1 is fixed (stabilized) on the action \mathbf{C}'_2 (eq. 6), the local symmetry of the orbit \mathcal{B} is determined to be \mathbf{C}'_2 . Thereby, the orbit \mathcal{B} is concluded to be governed by the CR $\mathbf{D}_{2d}/(\mathbf{C}'_2)$. Strictly speaking, the segments \mathcal{B}_1 and \mathcal{B}_3 are fixed on the action \mathbf{C}'_2 (eq. 6), while the segments \mathcal{B}_2 and \mathcal{B}_4 are fixed on the action \mathbf{C}''_2 (eq. 6). Because \mathbf{C}'_2 and \mathbf{C}''_2 are conjugate within \mathbf{D}_{2d} , they are regarded as being equivalent in this treatment.

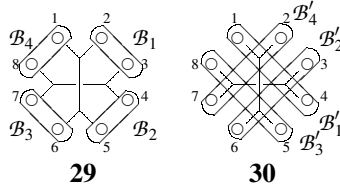


Figure 10: Segmentation patterns to generate orbits of \mathbf{C}'_2 -segments in the regular body (11) for illustrating the CR $\mathbf{D}_{2d}/(\mathbf{C}'_2)$.

The action of each operation of \mathbf{D}_{2d} (eq. 1) causes a permutation of the four segments of \mathcal{B} (29). Thereby, we can obtain the following permutations (as products of cycles) for the respective operations:

$$I \sim \begin{pmatrix} \mathcal{B}_1 & \mathcal{B}_2 & \mathcal{B}_3 & \mathcal{B}_4 \\ \mathcal{B}_1 & \mathcal{B}_2 & \mathcal{B}_3 & \mathcal{B}_4 \end{pmatrix} = (1)(2)(3)(4) \quad (31)$$

$$\mathbf{C}_{2(3)} \sim \begin{pmatrix} \mathcal{B}_1 & \mathcal{B}_2 & \mathcal{B}_3 & \mathcal{B}_4 \\ \mathcal{B}_3 & \mathcal{B}_4 & \mathcal{B}_1 & \mathcal{B}_2 \end{pmatrix} = (1\ 3)(2\ 4) \quad (32)$$

$$\mathbf{C}_{2(1)} \sim \begin{pmatrix} \mathcal{B}_1 & \mathcal{B}_2 & \mathcal{B}_3 & \mathcal{B}_4 \\ \mathcal{B}_1 & \mathcal{B}_4 & \mathcal{B}_3 & \mathcal{B}_2 \end{pmatrix} = (1)(2\ 4)(3) \quad (33)$$

$$\mathbf{C}_{2(2)} \sim \begin{pmatrix} \mathcal{B}_1 & \mathcal{B}_2 & \mathcal{B}_3 & \mathcal{B}_4 \\ \mathcal{B}_3 & \mathcal{B}_2 & \mathcal{B}_1 & \mathcal{B}_4 \end{pmatrix} = (1\ 3)(2)(4) \quad (34)$$

$$\sigma_{d(1)} \sim \begin{pmatrix} \mathcal{B}_1 & \mathcal{B}_2 & \mathcal{B}_3 & \mathcal{B}_4 \\ \overline{\mathcal{B}_4} & \overline{\mathcal{B}_3} & \overline{\mathcal{B}_1} & \overline{\mathcal{B}_2} \end{pmatrix} = \overline{(1\ 4)(2\ 3)} \quad (35)$$

$$\sigma_{d(2)} \sim \begin{pmatrix} \mathcal{B}_1 & \mathcal{B}_2 & \mathcal{B}_3 & \mathcal{B}_4 \\ \overline{\mathcal{B}_2} & \overline{\mathcal{B}_1} & \overline{\mathcal{B}_4} & \overline{\mathcal{B}_3} \end{pmatrix} = \overline{(1\ 2)(3\ 4)} \quad (36)$$

$$S_4 \sim \begin{pmatrix} \mathcal{B}_1 & \mathcal{B}_2 & \mathcal{B}_3 & \mathcal{B}_4 \\ \overline{\mathcal{B}_2} & \overline{\mathcal{B}_3} & \overline{\mathcal{B}_4} & \overline{\mathcal{B}_1} \end{pmatrix} = \overline{(1\ 2\ 3\ 4)} \quad (37)$$

$$S_4^3 \sim \begin{pmatrix} \mathcal{B}_1 & \mathcal{B}_2 & \mathcal{B}_3 & \mathcal{B}_4 \\ \overline{\mathcal{B}_4} & \overline{\mathcal{B}_1} & \overline{\mathcal{B}_2} & \overline{\mathcal{B}_3} \end{pmatrix} = \overline{(1\ 4\ 3\ 2)}. \quad (38)$$

The set of the permutations (eqs. 31—38) is a concrete form of the CR $\mathbf{D}_{2d}/(\mathbf{C}'_2)$, which is equivalent to the corresponding CR which has been algebraically obtained by using a coset decomposition of \mathbf{D}_{2d} by \mathbf{C}'_2 , as discussed generally in Chapter 7 of Fujita's book [12].

Because \mathbf{D}_{2d} is achiral and \mathbf{C}'_2 is chiral, a $\mathbf{D}_{2d}/(\mathbf{C}'_2)$ -orbit is enantiospheric according to the criterion of Table 5. This CR corresponds to a sphericity index c_4 because of $|\mathbf{D}_{2d}|/|\mathbf{C}'_2| = 8/2 = 4$.

Exercise 6. Construct a permutation diagram for the orbit \mathcal{B} by using the segmentation pattern 29 (Fig. 10). Then, derive the permutations shown in eqs. 31–38.

The right segmentation pattern (30) of Fig. 10 shows another orbit of segments governed by the CR $\mathbf{D}_{2d}/(\mathbf{C}'_2)$, i.e., $\mathcal{B}' = \{\mathcal{B}'_1, \mathcal{B}'_2, \mathcal{B}'_3, \mathcal{B}'_4\}$, where we place $\mathcal{B}'_1 = \{1, 4\}$, and $\mathcal{B}'_2 = \{3, 6\}$, $\mathcal{B}'_3 = \{5, 8\}$. $\mathcal{B}'_4 = \{2, 7\}$. The segments \mathcal{B}'_1 and \mathcal{B}'_3 are fixed on the action of \mathbf{C}'_2 (eq. 6), while the segments \mathcal{B}'_2 and \mathcal{B}'_4 are fixed on the action of \mathbf{C}''_2 (eq. 6), where \mathbf{C}'_2 and \mathbf{C}''_2 are conjugate within \mathbf{D}_{2d} .

Exercise 7. Construct a permutation diagram for the orbit \mathcal{B}' by using the segmentation pattern 30 (Fig. 10). Then, show permutations corresponding to the orbit \mathcal{B}' . Compare these permutations with eqs. 31–38.

4.2.3 Orbits of Segments Governed by the CR $\mathbf{D}_{2d}/(\mathbf{C}_2)$

Similarly, the four sets of two vertices as segments in 31 of Fig. 11, i.e., $C_1 = \{1, 5\}$, $C_2 = \{2, 6\}$, $C_3 = \{3, 7\}$, and $C_4 = \{4, 8\}$, are equivalent on the action of operations of \mathbf{D}_{2d} (eq. 1) so that they construct an orbit, i.e., $C = \{C_1, C_2, C_3, C_4\}$. Because the segment C_1 is fixed (stabilized) on the action \mathbf{C}_2 (eq. 5), the local symmetry of the orbit C is determined to be \mathbf{C}_2 . Thereby, the orbit C is concluded to be governed by the CR $\mathbf{D}_{2d}/(\mathbf{C}_2)$.

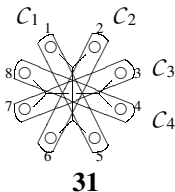


Figure 11: Segmentation pattern to generate an orbit of \mathbf{C}_2 -segments in the regular body (11) for illustrating the CR $\mathbf{D}_{2d}/(\mathbf{C}_2)$.

The action of each operation of \mathbf{D}_{2d} (eq. 1) causes a permutation of the four segments of C (31). Thereby, we can obtain the following permutations (as products of cycles) for the respective operations:

$$I, C_{2(3)} \sim \begin{pmatrix} C_1 & C_2 & C_3 & C_4 \\ C_1 & C_2 & C_3 & C_4 \end{pmatrix} = (1)(2)(3)(4) \quad (39)$$

$$C_{2(1)}, C_{2(2)} \sim \begin{pmatrix} C_1 & C_2 & C_3 & C_4 \\ C_4 & C_3 & C_2 & C_1 \end{pmatrix} = (1\ 4)(2\ 3) \quad (40)$$

$$\sigma_{d(1)}, \sigma_{d(2)} \sim \begin{pmatrix} C_1 & C_2 & C_3 & C_4 \\ \overline{C_2} & \overline{C_1} & \overline{C_4} & \overline{C_3} \end{pmatrix} = \overline{(1\ 2)(3\ 4)} \quad (41)$$

$$S_4, S_4^3 \sim \begin{pmatrix} C_1 & C_2 & C_3 & C_4 \\ \overline{C_3} & \overline{C_4} & \overline{C_1} & \overline{C_2} \end{pmatrix} = \overline{(1\ 3)(2\ 4)} \quad (42)$$

The set of the permutations (eqs. 39–42) is a concrete form of the CR $\mathbf{D}_{2d}/(\mathbf{C}_2)$, which is equivalent to the corresponding CR which has been algebraically obtained by using a coset decomposition of \mathbf{D}_{2d} by \mathbf{C}_2 , as discussed generally in Chapter 7 of Fujita’s book [12].

Because \mathbf{D}_{2d} is achiral and \mathbf{C}_2 is chiral, a $\mathbf{D}_{2d}/(\mathbf{C}_2)$ -orbit is enantiospheric according to the criterion of Table 5. This CR corresponds to a sphericity index c_4 because of $|\mathbf{D}_{2d}|/|\mathbf{C}_2| = 8/2 = 4$.

Exercise 8. Construct a permutation diagram for the orbit \mathcal{C} by using the segmentation pattern **31** (Fig. 11). Then, derive the permutations shown in eqs. 39–42.

4.2.4 Orbits of Segments Governed by the CR $\mathbf{D}_{2d}(/C_{2v})$

Similarly, the two sets of four vertices as segments in **32** of Fig. 12, i.e., $\mathcal{D}_1 = \{1, 2, 5, 6\}$ and $\mathcal{D}_2 = \{3, 4, 7, 8\}$, are equivalent on the action of operations of \mathbf{D}_{2d} (eq. 1) so that they construct an orbit, i.e., $\mathcal{D} = \{\mathcal{D}_1, \mathcal{D}_2\}$. Because the segment \mathcal{D}_1 is fixed (stabilized) on the action \mathbf{C}_{2v} (eq. 3), the local symmetry of the orbit \mathcal{D} is determined to be \mathbf{C}_{2v} . Thereby, the orbit \mathcal{D} is concluded to be governed by the CR $\mathbf{D}_{2d}(/C_{2v})$.

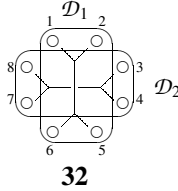


Figure 12: Segmentation pattern to generate an orbit of \mathbf{C}_{2v} -segments in the regular body (**11**) for illustrating the CR $\mathbf{D}_{2d}(/C_{2v})$.

The action of each operation of \mathbf{D}_{2d} (eq. 1) causes a permutation of the two segments of \mathcal{D} (**32**). Thereby, we can obtain the following permutations (as products of cycles) for the respective operations:

$$I, C_{2(3)} \sim \begin{pmatrix} \mathcal{D}_1 & \mathcal{D}_2 \\ \mathcal{D}_1 & \mathcal{D}_2 \end{pmatrix} = (1)(2) \quad (43)$$

$$C_{2(1)}, C_{2(2)} \sim \begin{pmatrix} \mathcal{D}_1 & \mathcal{D}_2 \\ \mathcal{D}_2 & \mathcal{D}_1 \end{pmatrix} = (1\ 2) \quad (44)$$

$$\sigma_{d(1)}, \sigma_{d(2)} \sim \begin{pmatrix} \mathcal{D}_1 & \mathcal{D}_2 \\ \overline{\mathcal{D}_1} & \overline{\mathcal{D}_2} \end{pmatrix} = \overline{(1)(2)} \quad (45)$$

$$S_4, S_4^3 \sim \begin{pmatrix} \mathcal{D}_1 & \mathcal{D}_2 \\ \overline{\mathcal{D}_2} & \overline{\mathcal{D}_1} \end{pmatrix} = \overline{(1\ 2)} \quad (46)$$

The set of the permutations (eqs. 43–46) is a concrete form of the CR $\mathbf{D}_{2d}(/C_{2v})$, which is equivalent to the corresponding CR which has been algebraically obtained by using a coset decomposition of \mathbf{D}_{2d} by \mathbf{C}_{2v} , as discussed generally in Chapter 7 of Fujita’s book [12].

Because both \mathbf{D}_{2d} and \mathbf{C}_{2v} is achiral, a $\mathbf{D}_{2d}(/C_{2v})$ -orbit is homospheric according to the criterion of Table 5. This CR corresponds to a sphericity index a_2 because of $|\mathbf{D}_{2d}|/|\mathbf{C}_{2v}| = 8/4 = 2$.

Exercise 9. Construct a permutation diagram for the orbit \mathcal{D} by using the segmentation pattern **32** (Fig. 12). Then, derive the permutations shown in eqs. 43–46.

4.2.5 Orbits of Segments Governed by the CR $\mathbf{D}_{2d}(/D_2)$

Similarly, the two sets of four vertices as segments in **33** of Fig. 13, i.e., $\mathcal{E}_1 = \{1, 4, 5, 8\}$ and $\mathcal{E}_2 = \{2, 3, 6, 7\}$, are equivalent on the action of operations of \mathbf{D}_{2d} (eq. 1) so that they construct

an orbit, i.e., $\mathcal{E} = \{\mathcal{E}_1, \mathcal{E}_2\}$. Because the segment \mathcal{E}_1 is fixed (stabilized) on the action \mathbf{D}_2 (eq. 2), the local symmetry of the orbit \mathcal{E} is determined to be \mathbf{D}_2 . Thereby, the orbit \mathcal{E} is concluded to be governed by the CR $\mathbf{D}_{2d}(\mathbf{D}_2)$.

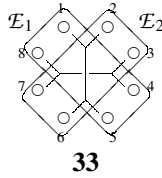


Figure 13: Segmentation pattern to generate an orbit of \mathbf{D}_2 -segments in the regular body (11) for illustrating the CR $\mathbf{D}_{2d}(\mathbf{D}_2)$.

The action of each operation of \mathbf{D}_{2d} (eq. 1) causes a permutation of the two segments of \mathcal{E} (33). Thereby, we can obtain the following permutations (as products of cycles) for the respective operations:

$$I, C_{2(3)}, C_{2(1)}, C_{2(2)} \sim \begin{pmatrix} \mathcal{E}_1 & \mathcal{E}_2 \\ \mathcal{E}_1 & \mathcal{E}_2 \end{pmatrix} = (1)(2) \quad (47)$$

$$\sigma_{d(1)}, \sigma_{d(2)}, S_4, S_4^3 \sim \begin{pmatrix} \mathcal{E}_1 & \mathcal{E}_2 \\ \overline{\mathcal{E}_2} & \overline{\mathcal{E}_1} \end{pmatrix} = \overline{(1\ 2)} \quad (48)$$

The set of the permutations (eqs. 47 and 48) is a concrete form of the CR $\mathbf{D}_{2d}(\mathbf{D}_2)$, which is equivalent to the corresponding CR which has been algebraically obtained by using a coset decomposition of \mathbf{D}_{2d} by \mathbf{D}_2 , as discussed generally in Chapter 7 of Fujita's book [12].

Because \mathbf{D}_{2d} is achiral and \mathbf{D}_2 is chiral, a $\mathbf{D}_{2d}(\mathbf{D}_2)$ -orbit is enantiospheric according to the criterion of Table 5. This CR corresponds to a sphericity index c_2 because of $|\mathbf{D}_{2d}|/|\mathbf{D}_2| = 8/4 = 2$.

Exercise 10. Construct a permutation diagram for the orbit \mathcal{E} by using the segmentation pattern 33 (Fig. 13). Then, derive the permutations shown in eqs. 47 and 48.

4.2.6 Orbits of Segments Governed by the CR $\mathbf{D}_{2d}(\mathbf{S}_4)$

Similarly, the two sets of four vertices as segments in 34 of Fig. 14, i.e., $\mathcal{F}_1 = \{1, 3, 5, 7\}$ and $\mathcal{F}_2 = \{2, 4, 6, 8\}$, are equivalent on the action of operations of \mathbf{D}_{2d} (eq. 1) so that they construct an orbit, i.e., $\mathcal{F} = \{\mathcal{F}_1, \mathcal{F}_2\}$. Because the segment \mathcal{F}_1 is fixed (stabilized) on the action \mathbf{S}_4 (eq. 4), the local symmetry of the orbit \mathcal{F} is determined to be \mathbf{S}_4 . Thereby, the orbit \mathcal{F} is concluded to be governed by the CR $\mathbf{D}_{2d}(\mathbf{S}_4)$.

The action of each operation of \mathbf{D}_{2d} (eq. 1) causes a permutation of the two segments of \mathcal{F} (34). Thereby, we can obtain the following permutations (as products of cycles) for the respective operations:

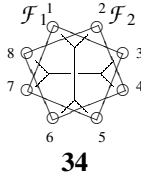


Figure 14: Segmentation pattern to generate an orbit of S_4 -segments in the regular body (11) for illustrating the CR $\mathbf{D}_{2d}(/S_4)$.

$$I, C_{2(3)} \sim \begin{pmatrix} \mathcal{F}_1 & \mathcal{F}_2 \\ \mathcal{F}_1 & \mathcal{F}_2 \end{pmatrix} = (1)(2) \quad (49)$$

$$C_{2(1)}, C_{2(2)} \sim \begin{pmatrix} \mathcal{F}_1 & \mathcal{F}_2 \\ \mathcal{F}_2 & \mathcal{F}_1 \end{pmatrix} = (12) \quad (50)$$

$$\sigma_{d(1)}, \sigma_{d(2)} \sim \begin{pmatrix} \mathcal{F}_1 & \mathcal{F}_2 \\ \overline{\mathcal{F}_2} & \overline{\mathcal{F}_1} \end{pmatrix} = \overline{(12)} \quad (51)$$

$$S_4, S_4^3 \sim \begin{pmatrix} \mathcal{F}_1 & \mathcal{F}_2 \\ \overline{\mathcal{F}_1} & \overline{\mathcal{F}_2} \end{pmatrix} = \overline{(1)(2)} \quad (52)$$

The set of the permutations (eqs. 49—52) is a concrete form of the CR $\mathbf{D}_{2d}(/S_4)$, which is equivalent to the corresponding CR which has been algebraically obtained by using a coset decomposition of \mathbf{D}_{2d} by S_4 , as discussed generally in Chapter 7 of Fujita's book [12].

Because both \mathbf{D}_{2d} and S_4 is achiral, a $\mathbf{D}_{2d}(/S_4)$ -orbit is homospheric according to the criterion of Table 5. This CR corresponds to a sphericity index a_2 because of $|\mathbf{D}_{2d}|/|S_4| = 8/4 = 2$.

Exercise 11. Construct a permutation diagram for the orbit \mathcal{F} by using the segmentation pattern 34 (Fig. 14). Then, derive the permutations shown in eqs. 49–52.

4.2.7 Orbit of a Segment Governed by the CR $\mathbf{D}_{2d}(/D_{2d})$

This is a trivial case. The corresponding segment pattern contains all of the eight positions. i.e., $\mathcal{G}_1 = \{1, 2, 3, 4, 5, 6, 7, 8\}$. Because all of the symmetry operations of \mathbf{D}_{2d} transform \mathcal{G}_1 into \mathcal{G}_1 itself (or $\overline{\mathcal{G}_1}$), the following trivial permutations are obtained:

$$I, C_{2(3)}, C_{2(1)}, C_{2(2)} \sim \begin{pmatrix} \mathcal{G}_1 \\ \mathcal{G}_1 \end{pmatrix} = (1) \quad (53)$$

$$\sigma_{d(1)}, \sigma_{d(2)}, S_4, S_4^3 \sim \begin{pmatrix} \mathcal{G}_1 \\ \overline{\mathcal{G}_1} \end{pmatrix} = \overline{(1)} \quad (54)$$

The set of the permutations (eqs. 53 and 54) is a concrete form of the CR $\mathbf{D}_{2d}(/D_{2d})$. Because the achiral point group \mathbf{D}_{2d} appears as the global and the local symmetry, a $\mathbf{D}_{2d}(/D_{2d})$ -orbit is homospheric according to the criterion of Table 5. This CR corresponds to a sphericity index a_1 because of $|\mathbf{D}_{2d}|/|\mathbf{D}_{2d}| = 8/8 = 1$.

Exercise 12. Show a segmentation pattern for representing the orbit \mathcal{G} governed by the CR $\mathbf{D}_{2d}(/D_{2d})$. Thereby, construct a permutation diagram for the orbit \mathcal{G} . Then, derive the permutations shown in eqs. 53 and 54.

4.2.8 General Procedure for Obtaining CRs

The diagrammatical procedure described in the preceding paragraphs can be generalized to obtain any CRs. Thus, any CR can be obtained stepwise as follows:

1. **Select a regular body** for $\mathbf{G}/(\mathbf{C}_1)$. This step is somewhat experiential. By starting from a known skeleton of \mathbf{G} , an appropriate substitution would generate a regular body. For example, compare the allene skeleton **1** of Fig. 1 with the regular body **11** of Fig. 6.
2. **Construct a permutation diagram** for \mathbf{G} . To accomplish this step, let every symmetry operations of \mathbf{G} act on the regular body to give permuted transformulas, which construct a permutation diagram such as Fig. 7.
3. **Select an orbit of segments** in the regular body, where the local symmetry of each segment is \mathbf{H} (a subgroup of \mathbf{G}). Concretely speaking, select a segmentation pattern such as **20** shown Fig. 8.
4. **Superpose the segmentation pattern onto the permutation diagram**. This operation means that every symmetry operations of \mathbf{G} act on the orbit to give permuted transformulas, which construct such a diagram as shown in Fig. 9.
5. **Compare each resulting transformula with the original one** in the resulting diagram to give a permutation of $\mathbf{G}/(\mathbf{H})$. For example, the original transformula **20** is compared with **22–28** in Fig. 9.

Following this stepwise procedure, any CRs are available systematically in a diagrammatical way. They have been proved to be identical with the corresponding CRs that are obtained algebraically [12].

Exercise 13. Show a regular body for the point group \mathbf{T}_d by starting from adamantane. See Ref. [32].

Exercise 14. Show another regular body for \mathbf{D}_{2d} by examining adamantane-2,6-dione. See Ref. [16]. This exercise shows another methodology of constructing a regular body of a given symmetry, where a skeleton belonging to a supergroup (e.g., adamantane of \mathbf{T}_d -symmetry) is subduced into another skeleton of the required symmetry (e.g., adamantane-2,6-dione of \mathbf{D}_{2d}). Compare this methodology with the present one based on the derivation of symmetry conservation (e.g., from the allene skeleton of \mathbf{D}_{2d} -symmetry (**1** in Fig. 1) to the regular body of \mathbf{D}_{2d} -symmetry (**11** in Fig. 6)).

5 Mathematical Models into Chemical Structures

Mathematical concepts in their original forms are not always applicable to chemical problems. Thus, the concept of *segments* described in Section 4 still remains to be a mathematical model, although it has been defined intuitively and diagrammatically. This section deals with *ligands*, *proligands*, and *atoms* as more chemical objects and links them with *segments*, so that the concept of CRs based on the concept of segments is restated on the basis of chemical concepts of ligands etc. This means that the items discussed diagrammatically in Sections 2 and 3 are provided with a mathematical foundation by means of the diagrammatical approach described in Section 4.

5.1 Ligands as Special Segments

5.1.1 Ligands in a Molecule

By comparing between **1** (Fig. 1) and **20** (Fig. 8), one can find that the orbit of the four hydrogen atoms in **1** and the orbit of the four segments (\mathcal{A}_1 to \mathcal{A}_4) in **20** are both governed by the CR $\mathbf{D}_{2d}/\mathbf{C}_s$ and that the four carbon atoms in the cyclopropane rings of **20** is also governed by the same CR $\mathbf{D}_{2d}/\mathbf{C}_s$. It follows that the four combined segments derived from \mathcal{A}_i ($i = 1, 2, 3, 4$) and each root carbon atom, i.e., $\text{CH}^{(1)}\text{H}^{(2)}$ for \mathcal{A}_1 , $\text{CH}^{(3)}\text{H}^{(4)}$ for \mathcal{A}_2 , $\text{CH}^{(5)}\text{H}^{(6)}$ for \mathcal{A}_3 , and $\text{CH}^{(7)}\text{H}^{(8)}$ for \mathcal{A}_4 , construct an orbit governed by the same CR $\mathbf{D}_{2d}/\mathbf{C}_s$. Because such combined segments have a chemical meaning, they are called *ligands*. Although the expression “chemical meaning” is used as having rather broad connotation, one may consider that the term “ligand” designates an object consisting of atoms, which is meaningful even when isolated.

Each of the ligands CH_2 belongs to the local symmetry \mathbf{C}_s , which appears in the CR $\mathbf{D}_{2d}/\mathbf{C}_s$. The two hydrogen atoms in each ligand CH_2 can be considered to construct a sub-orbit governed by $\mathbf{C}_s/\mathbf{C}_1$, if one pay an attention to the ligand. On the other hand, the two hydrogen atoms in each ligand CH_2 are part of the eight hydrogen atoms of **20**, which construct an orbit governed by the CR $\mathbf{D}_{2d}/\mathbf{C}_1$. Hence the successive symmetry degradation from \mathbf{D}_{2d} (total symmetry) to \mathbf{C}_1 (atom or position symmetry) via \mathbf{C}_s (ligand symmetry) corresponds to the combination of the CRs the CR $\mathbf{D}_{2d}/\mathbf{C}_s$ and the CR $\mathbf{C}_s/\mathbf{C}_1$ producing the total CR $\mathbf{D}_{2d}/\mathbf{C}_1$. The successive symmetry degradation has been discussed algebraically in Chapter 7 (especially Fig. 7.1) of Fujita’s book [12].

5.1.2 Ligands in Isolation

Although the CH_2 ligand belongs to \mathbf{C}_s when incorporated in **20** (Fig. 8), the ligand belongs to \mathbf{C}_{2v} when isolated, where the two hydrogen atoms of the CH_2 construct a two-membered orbit governed by the CR $\mathbf{C}_{2v}/\mathbf{C}_s$. The CH_2 -ligand of the \mathbf{C}_{2v} -symmetry is accommodated in **20** as a \mathbf{C}_s -ligand, where the \mathbf{C}_{2v} is restricted to the local symmetry \mathbf{C}_s . This process is represented by the subduction of the CR $\mathbf{C}_{2v}/\mathbf{C}_s$ to \mathbf{C}_s as follows:

$$\mathbf{C}_{2v}/\mathbf{C}_s \downarrow \mathbf{C}_s = \mathbf{C}_s/\mathbf{C}_1 \quad (55)$$

This restriction is here referred to as *ligand-symmetry restriction*. It should be noted that $\mathbf{C}_{2v}/\mathbf{C}_s$ in the left-hand side of eq. 55 is homospheric, while $\mathbf{C}_s/\mathbf{C}_1$ in the right-hand side of eq. 55 is enantiospheric.

5.1.3 Rotatable Ligands

The concept of ligand-symmetry restriction is useful to discuss rotatable ligands. Although this subject has been discussed in previous papers [33, 27] and Chapters 20 and 21 of Fujita’s book [12], illustrative examples suitable for the present context are useful to comprehend symmetrical properties during substitution processes.

Suppose that the four hydrogens of **1** are replaced by methyl ligands to produce tetramethylallene (**35**). Although this process is seemingly similar to the case of 5.1.2 in which the methylene ligands are fixed after accommodated in the molecule (**20**), the methyl ligands are *not* fixed so as to be rotatable after accommodated in the molecule (**35**).

The symmetry of each methyl belongs to \mathbf{C}_{3v} in isolation. After accommodated in **35**, it is controlled by the local symmetry \mathbf{C}_s derived from the CR $\mathbf{D}_{2d}/\mathbf{C}_s$. Thereby, the ligand-symmetry restriction takes place so as to be represented by the subduction of the CR $\mathbf{C}_{3v}/\mathbf{C}_s$

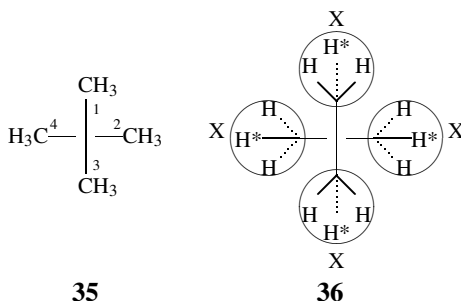


Figure 15: Methyl ligands as rotatable ligands in tetramethylallene (left) and its highest attainable symmetry (right).

to C_s as follows:

$$C_{3v}(/C_s) \downarrow C_s = C_s(/C_s) + C_s(/C_1) \quad (56)$$

By the free rotation around each C—C bond, the three hydrogen atoms of each methyl ligand are equivalent.

When such free rotation is restricted, they are fixed and divided into a two-membered orbit and a one-membered orbit according to eq. 56. This result can be confirmed by a fixed conformation having the highest attainable symmetry (**36**). In the fixed conformer (**36**), the four hydrogens with an asterisk constructs a homospheric four-membered orbit governed by the CR $D_{2d}(/C_s)$, which is derived from $D_{2d}(/C_s)$ (Table 6) and $C_s(/C_s)$ (eq. 56). On the other hand, the eight hydrogens without an asterisk in **36** construct an enantiospheric eight-membered orbit governed by the CR $D_{2d}(/C_1)$, which is derived from $D_{2d}(/C_s)$ (Table 6) and $C_s(/C_1)$ (eq. 56). Note that the $D_{2d}(/C_1)$ -orbit in the fixed conformer (**36**) symmetrically resembles the $D_{2d}(/C_1)$ -orbit in the regular body (**11**).

Exercise 15. Examine the symmetry of tetramethylmethane ($C(CH_3)_4$). Show its highest attainable symmetry in a similar way described for Fig. 15. See Ref. [27] and Chapter 21 of Fujita's book.

The ligand separation represented by eq. 56 can be explicitly realized by considering hydroxymethyl ligands in place of the methyl ligands, as shown in Fig. 16. The two hydrogens of the hydroxymethyl ligand is governed by the CR $C_s(/C_1)$ (eq. 56), while the hydroxy ligand is governed by the CR $C_s(/C_s)$ (eq. 56).

As for the corresponding fixed conformation having the highest attainable symmetry (**38**), the four hydroxy ligands constructs a homospheric four-membered orbit governed by the CR $D_{2d}(/C_s)$, which is derived from $D_{2d}(/C_s)$ (Table 6) and $C_s(/C_s)$ (eq. 56). On the other hand, the eight hydrogens in **38** construct an enantiospheric eight-membered orbit governed by the CR $D_{2d}(/C_1)$, which is derived from $D_{2d}(/C_s)$ (Table 6) and $C_s(/C_1)$ (eq. 56). Compare **36** and **38** to see the correspondence between asterisked hydrogens and hydroxyl ligands.

Exercise 16. Examine the symmetry of pentaerythritol ($C(CH_2OH)_4$). Show its highest attainable symmetry in a similar way described for Fig. 16. See Ref. [27] and Chapter 21 of Fujita's book.

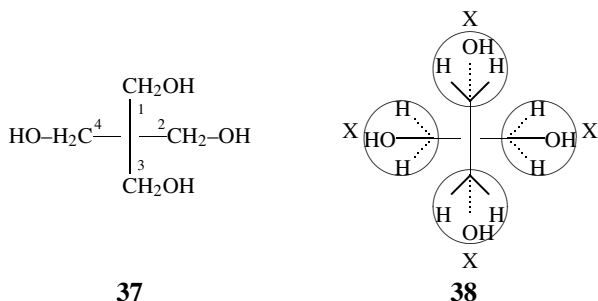


Figure 16: Hydroxymethyl ligands as rotatable ligands (left) and its highest attainable symmetry (right).

Let us next examine the substitution of chiral *R*- and *S*-chlorofluoromethyl ligands as shown in Fig. 17, where *R* and *S*-configurations are tentatively determined in terms of the priority $\text{Cl} > \text{F} > \text{H} > \text{null}$. This substitution gives a molecule **39**, which corresponds to **5** of S_4 -symmetry as a reference promolecule, if p and \bar{p} are substituted for *R*- and *S*-chlorofluoromethyl ligands. Each atom (Cl, F, or H) in an isolated chlorofluoromethyl ligand is governed by a respective $\text{CR } \text{C}_1$ ($/\text{C}_1$). Thereby, the four hydrogens (or chlorines or fluorines) in **39** construct a four-membered orbit governed by S_4 ($/\text{C}_1$).⁷

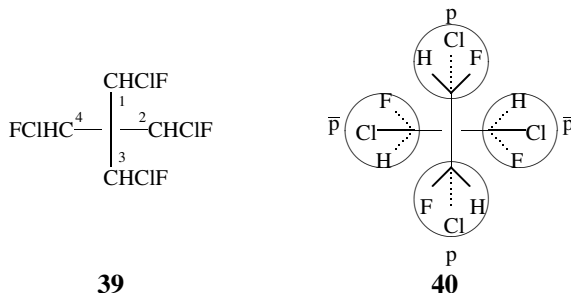


Figure 17: Chlorofluoromethyl ligands as rotatable ligands (left) and its highest attainable symmetry (right).

⁷If we consider the promolecule **1** having $\text{D}_{2d}(/C_2)$ as a reference promolecule, the C_1 -symmetry of an *R*- or *S*-chlorofluoromethyl ligand is mismatched to the local symmetry C_s after accommodation in **39**. This means that the D_{2d} -symmetry of an allene molecule is influenced to be changed into S_4 . By this desymmetrization, the four hydrogens (or chlorines or fluorines) in **39** become to construct a four-membered orbit governed by S_4 ($/\text{C}_1$). To avoid such ambiguity in selecting a reference promolecule, such a reference molecule should be selected so as to conserve the sphericity in the conversion of a promolecule (**5** having an enantiospheric orbit) into a molecule (**39** having an enantiospheric orbit) if possible. Note that the conversion of a promolecule (**1** having a homospheric orbit) into a molecule (**39** having an enantiospheric orbit) does not conserve the sphericity.

Exercise 17. Examine the substitution of four *R*-chlorofluoromethyl ligands (or *S*-chlorofluoromethyl ligands) onto the four positions of allene. Compare this case with Fig. 17.

Exercise 18. Examine the symmetry of a methane derivative having two *R*-chlorofluoromethyl ligands and two *S*-chlorofluoromethyl ligands. Show its highest attainable symmetry in a similar way described for Fig. 17. See Fig. 21.1 of Fujita's book [12].

5.1.4 Chirality Fittingness and Symmetry Fittingness

Suppose that the four hydrogens of a methane molecule, which belong to a $T_d(/C_{3v})$ -orbit, are replaced by four hydroxymethyl ligands (CH_2OH) of C_s -symmetry. This process generates pentaerythritol, i.e., $C(CH_2OH)_4$, which belongs to D_{2d} at the highest attainable symmetry in spite of the vacancy at the D_{2d} -symmetry shown in Fig. 4. This is because the C_s -symmetry of each hydroxymethyl ligand (CH_2OH) is mismatched to the local symmetry (C_{3v}) of the $T_d(/C_{3v})$ -orbit. Thereby, the $T_d(/C_{3v})$ -orbit is converted into a $D_{2d}/(C_s)$ -orbit so that the latter local symmetry (C_s) becomes suitable for the C_s -symmetry of each hydroxymethyl ligand (CH_2OH).

This kind of desymmetrizations have been discussed in terms of “matched” and “mismatched” molecules in a previous paper [27] and Chapter 21 of Fujita's book [12]. They can be summarized by a term *symmetry fittingness*, which is here coined by analogy to *chirality fittingness*. It should be noted that the concept of *symmetry fittingness* is concerned with **molecules** with ligands, because *CRs* are used to discuss stereochemistry in molecule. On the other hand, the concept of *chirality fittingness* is concerned with **promolecules** as well as *molecules*, because *sphericities* are used to discuss stereochemistry in molecule (even in promolecule level).

5.2 Atoms and Proligands as Special Segments

An atom can be regarded as an extreme case in which all the objects of a segment coincides to give a single object. In the USCI approach, strictly speaking, a *proligand* is regarded as an extreme case in which all the objects of a segment coincides to give a single object. Then, an atom is further regarded as a special case of such proligands. Sections 2 and 3 have provided us with various examples of such extreme cases.

Such extreme cases are sometimes forbidden, as discussed previously in a paper [30] and Section 7.2 of Fujita's book [12]. As a result, some *CRs* are forbidden to specify orbits in a molecule. Among the *CRs* of the D_{2d} -symmetry, for example, $D_{2d}/(C_2)$ (giving the same atom as derived by $D_{2d}/(C_{2v})$), $D_{2d}/(S_4)$ (giving the same atom as derived by $D_{2d}/(D_{2d})$), an $D_{2d}/(D_2)$ (giving the same atom as derived by $D_{2d}/(D_{2d})$) are forbidden, as summarized in Appendix C of Fujita's book [12].

Except such forbidden cases, the remaining *CRs*, i.e., $D_{2d}/(C_1)$, $D_{2d}/(C_s)$, $D_{2d}/(C'_2)$, $D_{2d}/(C_{2v})$, and $D_{2d}/(D_{2d})$, can appear to specify orbits in a molecule. For example, $D_{2d}/(C_s)$ (the orbit of four hydrogens) and $D_{2d}/(C_{2v})$ (the orbit of two terminal atoms of the allene axis) appear, as shown in Table 6. The *CR* $D_{2d}/(D_{2d})$ governs a one-membered orbit consisting of the central atom of the allene axis ($C=C^*=C$). The *CR* $D_{2d}/(C_1)$ governs an eight-membered orbit in the regular body (**11**).

The *CR* $D_{2d}/(C'_2)$ is not realized as an orbit of atoms (or proligands) if we start from the present regular body. However, another regular body based on adamantane-2,6-dione can be considered, where the eight hydrogens at the bridge methylenes constructs a $D_{2d}/(C_1)$ -orbit (cf. Exercise 14). The four methylene carbons at the bridge positions of adamantane-2,6-dione

construct a four-membered orbit governed by $D_{2d}(/C_2')$, as has been discussed in Example 10.1 of Fujita's book [12].

6 Subductive Derivation

6.1 Subductive Derivation Based on a Regular Body

By inspection of Figs. 8 and 10–14, one can find a general method of deriving molecules of given symmetries. For example, by placing ● (in place of ○) on the positions of a segment (e.g., \mathcal{A}_1) in **20** (Fig. 8), a C_s -molecule **41** can be derived, as shown in Fig. 18. Similarly, another C_s -molecule **42** (Fig. 18) can be derived by placing ● on the positions of a segment (\mathcal{A}'_1) in **21** (Fig. 8). According to this method, Figs. 10–14 generate molecules of respective symmetries. This type of derivation extensively discussed in terms of *subductive derivation* [32].

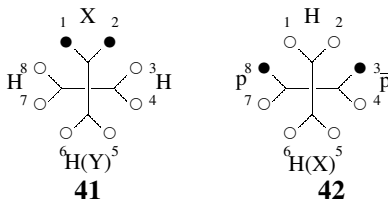


Figure 18: C_s -molecules generated from the regular body (**11**). Compare these molecules with the C_s -segments shown in Fig. 8. And compare these molecules with the C_s -molecule shown in Fig. 3, where the modes of segmentation represented by the symbols H, X, Y, p, and \bar{p} are taken into consideration.

It is informative to depict the resulting molecules in a subduction diagram, as shown in Fig. 19. The USCI-CF and the USCI listed below the formula of each molecule indicate the division of the eight positions to orbits. For example, there emerged four two-membered enantiospheric orbits (i.e., $\{1,2\}$, $\{3,8\}$ $\{4,7\}$, and $\{5,6\}$) in **41** (Fig. 18) in agreement with the USCI-CF (i.e., c_2^4) shown in Fig. 19. The same molecule as **41** is listed in an alternative expression (**48**) in Fig. 19, which is convenient to explain the relationship between Fig. 19 and Fig. 3 (see 6.2). Of course, the other one **42** may be depicted as a C_s -molecule in Fig. 19.

Similarly, the division of the positions into orbits occurs in agreement with the USCI-CF attached to each formula, as shown in Fig. 19.

6.2 Subductive Derivation From Various Viewpoints

The comparison of **41** (Fig. 18) with the C_s -promolecule (**9**) listed in Fig. 3 provides us with another view on ligand substitutions. Let us represent ligands in **41** by the symbol $C\{1,2\}$, etc. Then, the ligands $C\{3,4\}$ and $C\{7,8\}$ in **41** correspond to the two hydrogen atoms of **9**, while $C\{1,2\}$ and $C\{5,6\}$ can be correlated to X and Y, respectively. The symbols H, H, X, and Y are added in the formula **41** to show this correspondence. The sphericity index c_2 is assigned to the two-membered enantiospheric orbit of ligands $C\{3,4\}$ and $C\{7,8\}$ in **41**, while a_1 is assigned

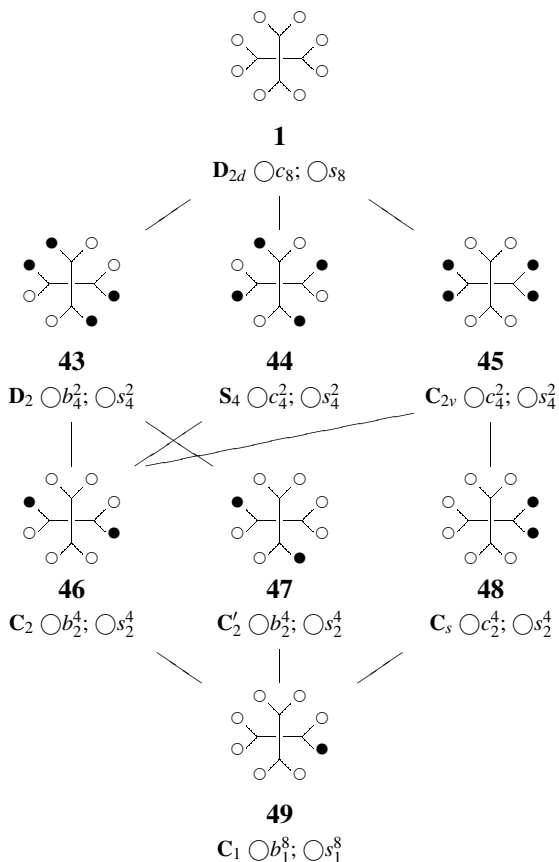


Figure 19: Subduction diagram with USCIs and USCI-CFs for testing the existence or nonexistence of derivatives during vertex substitution of the regular body (**1**). The symbol \bigcirc shows the existence of a desymmetrized molecule. This subduction diagram is concerned with the C_1 in agreement with no segmentation.

to each one-membered homospheric orbit of a ligand $C\{1,2\}$ or $C\{5,6\}$. It follows that the USCI-CF $a_1^2 c_2$ is assigned to the ligands of **41**.

On the other hand, four ligands in the other C_s -molecule (**42**) can be regarded as proligands (H, H(X), p, and \bar{p}), as added in the formula (**42**), where the ligands $C\{3,4\}$ and $C\{7,8\}$ correspond to \bar{p} and p while $C\{1,2\}$ and $C\{5,6\}$ corresponds to H and H (X). Note that the H and the H(X) belongs respectively to one-membered orbits. The segmentation means that the sphericity index c_2 is assigned to the two-membered enantiospheric orbit of ligands $C\{3,4\}$ (\bar{p}) and $C\{7,8\}$ (p) in **42**, while a_1 is assigned to each one-membered homospheric orbit of a ligand $C\{1,2\}$ (H) or $C\{5,6\}$ (H or X). It follows that the USCI-CF $a_1^2 c_2$ is assigned to the proligands

of **42**.

In summary, the same transformulas are concurrently regarded as being generated by two modes of substitution.

1. From one viewpoint, the USCI-CF c_2^4 should be assigned to **41** (or **42**) if the eight positions of **41** (or **42**) are not segmented to ligands. By this viewpoint, there emerged four two-membered enantiospheric orbits (i.e., {1,2}, {3,8} {4,7}, and {5,6}) in **41** (or **42**), each of which corresponds to the sphericity index c_2 so as to give the USCI-CF c_2^4 .
2. From the other viewpoint in which the eight positions of **41** (or **42**) are segmented to ligands, there appear a one-membered orbit of C{1,2} (for a_1), a one-membered orbit of C{5,6} (for a_1), and a two-membered orbit of {C{3,4} and C{7,8}} (for c_2) in agreement with the USCI-CF $a_1^2c_2$, as shown in Fig. 18,

The C_2' -molecule (**47**) depicted in Fig. 19 is derived from **30** (Fig. 10). As shown in Fig. 20, the molecule (**47**) is regarded as being generated by substitution of the set of proligands {H, H, p, and p}, if the ligands C{1,2} and C{3,4} in **47** are symmetrically equalized to two hydrogens (as achiral proligands) and the ligands C{5,6} and C{7,8} are symmetrically equalized to two chiral proligands (p). Because the C_2' is chiral, the corresponding enantiomer (**47**) can be generated by starting also from **30** where the substitution corresponds to the proligand set {H, H, \bar{p} , and \bar{p} }, as shown in Fig. 20.

As shown in Fig. 20, another C_2' -molecule (**50**) and its enantiomer (**50**) can be derived from **29** (Fig. 10). Each of the molecules is regarded as being generated by substitution of {H, H, \bar{p} , and \bar{p} } or {H, H, p, and p}.

A further C_2' -molecule (**51**) and its enantiomer (**51**) can be derived by combining **29** with **30** (Fig. 10). Both of the molecules are regarded as being generated by substitution of {H, H, X, and X}.

Again, the same transformulas are concurrently regarded as being generated by two modes of substitution.

1. If the eight positions of **47** (or **50** or **42**) are not segmented to ligands, there emerged four two-membered enantiospheric orbits (i.e., {2,3}, {1,4} {5,8}, and {6,7}) of **47** (or **50** or **42**), which are in agreement with the USCI-CF b_2^4 . The same situation holds true for the C_2' -molecule (**51**).
2. On the other hand, if the modes of segmentation are taken into consideration, the resulting ligands C{1,2}, C{3,4}, C{5,6} and C{7,8} in **47** (or **50** or **42**) are controlled in agreement with the common USCI-CF, i.e., $a_1^2c_2$. The same situation holds true for the C_2' -molecule (**51**).

This type of segmentations is applicable to any of the molecules listed in Fig. 19. Thus, the procedure of the segmentations shown in Fig. 18 (C_s) and 20 (C_2') is repeated to every remaining molecules. This means that the mode of segmentation depicted for **20** (Fig. 8) is superposed onto each formula listed in Fig. 19. Thereby, we obtain Fig. 21 as a subduction diagram, where the C_s -molecule (**41**) shown in Fig. 18 and the C_2' -molecule (**47**) shown in Fig. 20 appear as **57** and **56**, respectively. Because the methodology of superposition is versatile in discussing symmetry, it is here called *segmentation-pattern superposition*.

Obviously, Fig. 21 has the same context as Fig. 3, which is concerned with a $D_{2d}(/C_s)$ -orbit. To show the correspondence clearly, the proligand symbols (H, X, Y, p, and \bar{p}) are added

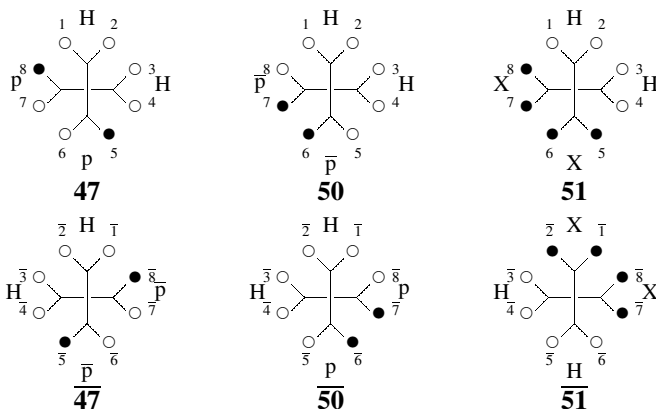


Figure 20: C_2' -molecules generated from the regular body (**11**). Compare these molecules with the C_2' -segments shown in Fig. 10.

in Fig. 21. Note that, although the C_2' -molecule (**8**) shown in Fig. 3 corresponds to **51**, Fig. 21 contains an alternative molecule (**56**) for the sake of consistency between Fig. 21 and Fig. 19 (see also Fig. 20).

The procedure for obtaining the subduction diagram (Fig. 21) from Fig. 19 can be generalized easily in terms of segmentation-pattern superposition. For example, the mode of segmentation shown in Fig. 10 (for the C_2' -segment) is superposed onto Fig. 19 to give a subduction diagram of a $D_{2d}(/C_2')$ -orbit. Similarly, Figs. 11 (for the C_2 -segment), 12 (for the C_{2v} -segment), 13 (for the D_2 -segment), and 14 (for the S_4 -segment) can be used to generate subduction diagrams corresponding to $D_{2d}(/C_2)$, $D_{2d}(/C_{2v})$, $D_{2d}(/D_2)$, and $D_{2d}(/S_4)$.

Such subduction diagrams corresponding to CRs contain the modes of desymmetrization, which are represented by subductions of CRs. The next section will deal with the subduction diagrams more systematically.

Exercise 19. Following the superposition procedure described above (Fig. 19 + Fig. 8 \rightarrow Fig. 21), superpose the segmentation pattern shown in Fig. 10 (for the C_2' -segment) onto Fig. 19. Repeat the superposition procedure by using the following segmentation patterns: Figs. 11 (for the C_2 -segment), 12 (for the C_{2v} -segment), 13 (for the D_2 -segment), and 14 (for the S_4 -segment).

7 Diagrammatical Derivation of Subductions of CRs

The concept of *subductions of CRs* has been proposed by Fujita [34] and discussed somewhat algebraically in Chapter 9 of Fujita's book [12]. This concept can be alternatively formulated by using the diagrammatical expressions of a regular body described in Section 4. This is the target of this section, where the concept of *assemblies of transformulas* is introduced to visualize subduction processes. Thereby, such subduction diagrams as discussed in Section 6 are diagrammatically provided with a mathematical foundation.

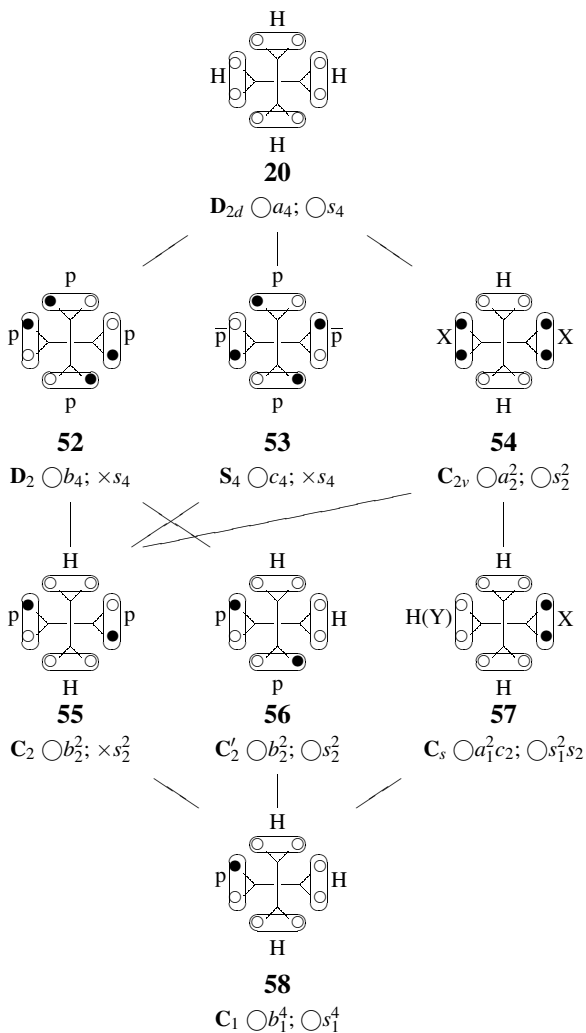


Figure 21: Subduction diagram with USCIs and USCI-CFs for testing the existence or nonexistence of derivatives during segment substitution of the segmented regular body (20). The symbol \circ shows the existence of a desymmetrized molecule, while \times shows non-existence. This subduction diagram is concerned with the CR $\mathbf{D}_{2d}(/C_s)$ according to the mode of segmentation shown in Fig. 8.

7.1 Subduction of the Regular Representation

First, the subduction of the regular representation is examined diagrammatically as an extreme case of coset representations. This diagrammatical examination results in an integrated comprehension of the segmentation patterns (Section 4) and the subductive derivation (Section 6).

Let us consider the permutations listed in Fig. 7, which correspond to the eight symmetry operations of \mathbf{D}_{2d} (eq. 1). By selecting **11** and **13**, the original \mathbf{D}_{2d} -symmetry is restricted to give $\mathbf{C}_s = \{I, \sigma_{d(1)}\}$ (eq. 7), as shown in Fig. 22. This process is called the *subduction of a coset representation* and designated by the symbol $\mathbf{D}_{2d}(/C_1) \downarrow C_s$. The resulting set of transformulas (**11** and **13**) is called an *assembly of transformulas*.

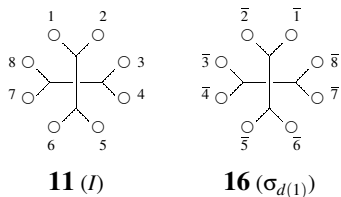


Figure 22: An assembly of two transformulas for the subduction $\mathbf{D}_{2d}(/C_1) \downarrow C_s = 4C_s(/C_1)$. Thereby, the eight-membered orbit \mathcal{R} is divided into four orbits, i.e., $\mathcal{R}_1 = \{1, 2\}$, $\mathcal{R}_2 = \{3, 8\}$, $\mathcal{R}_3 = \{4, 7\}$, and $\mathcal{R}_4 = \{5, 6\}$.

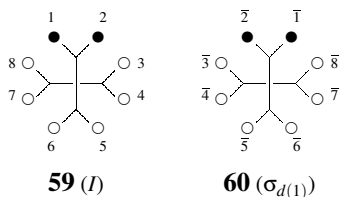


Figure 23: An assembly of two transformulas for representing an allene molecule generated by the subduction $\mathbf{D}_{2d}(/C_1) \downarrow C_s = 4C_s(/C_1)$. Among the resulting orbits ($\mathcal{R}_1 = \{1, 2\}$, $\mathcal{R}_2 = \{3, 8\}$, $\mathcal{R}_3 = \{4, 7\}$, and $\mathcal{R}_4 = \{5, 6\}$), the two positions of \mathcal{R}_1 occupied placed by different atoms (●). The two transformulas (**59** and **60**) are identical to give a single C_s -molecule (**41**).

As a result of this symmetry restriction, the original orbit $\mathcal{R} = \{1, 2, 3, 4, 5, 6, 7, 8\}$ no longer maintains its equivalence so that it is divided into several orbits. By the inspection of the two transformulas in Fig. 22, we can find the generation of four orbits, i.e., $\mathcal{R}_1 = \{1, 2\}$, $\mathcal{R}_2 = \{3, 8\}$, $\mathcal{R}_3 = \{4, 7\}$, and $\mathcal{R}_4 = \{5, 6\}$. This process corresponds to the selection of $I \sim (1)(2)(3)(4)(5)(6)(7)(8)$ (eq. 14) and $\sigma_{d(1)} \sim \overline{(1\ 2)(3\ 8)(4\ 7)(5\ 6)}$ (eq. 18), when we remember the concrete form of $\mathbf{D}_{2d}(/C_1)$ (eqs. 14–21).

Because the local symmetry of the object no. 1 in \mathcal{R}_1 is determined to be C_1 (Fig. 22), the orbit \mathcal{R}_1 is governed by the coset representation $C_s(/C_1)$. Obviously, the remaining orbits, \mathcal{R}_2 , \mathcal{R}_3 , and \mathcal{R}_4 , are also governed by the CR $C_s(/C_1)$. This result can be summarized by the following equation:

$$\mathbf{D}_{2d}(/C_1) \downarrow C_s = 4C_s(/C_1) \tag{57}$$

On the same line as an assembly containing the eight transformulas (11–19) shown in Fig. 7 represents a \mathbf{D}_{2d} -molecule (a regular body), the assembly of the transformulas (11 and 13) shown in Fig. 22 represents a \mathbf{C}_s -molecule, which can be regarded as a regular body with multiple regular representations, as shown in the right-hand side of eq. 57.

Exercise 20. Select assemblies of transformulas for other subgroups of \mathbf{D}_{2d} and get their subduction equations according to the above procedure for obtaining eq. 57 of the subgroup \mathbf{C}_s .

The result shown in eq. 57 can be extended to cover any regular representation $\mathbf{G}(/C_1)$, giving the following equation:

$$\mathbf{G}(/C_1) \downarrow \mathbf{G}_i = \frac{|\mathbf{G}|}{|\mathbf{G}_i|} \mathbf{G}_i(/C_1), \quad (58)$$

where \mathbf{G}_i is a subgroup of \mathbf{G} , as shown in Section 7.1 of Fujita's book [12].

The subduction process shown in Fig. 22 allows us to generate \mathbf{C}_s -transformulas by placing two atoms of the same kind on each of the resulting orbits (\mathcal{R}_1 , \mathcal{R}_2 , \mathcal{R}_3 , and \mathcal{R}_4). For example, the substitution of \mathcal{R}_1 shown in Fig. 22 generates an assembly of transformulas (59 and 60), as shown in Fig. 23. The resulting transformulas (59 and 60) are identical with each other when the numbering is disregarded so that the assembly of 59 and 60 indicates the occurrence of a single \mathbf{C}_s -molecule (41) of this type, which has already been studied in Fig. 18. In other words, the assembly of the two transformulas (59 and 60) characterizes the symmetry of a \mathbf{C}_s -molecule.

The result shown in eq. 57 can be generalized to cover any regular representation $\mathbf{G}(/C_1)$, giving eq. 58. Hence, the subduction result corresponds to the USCI-CF c_d^m (for an achiral \mathbf{G}) or b_d^m (for a chiral \mathbf{G}), where we place $d = |\mathbf{G}_i|$ and $m = |\mathbf{G}|/|\mathbf{G}_i|$. The USCI-CFs for $\mathbf{D}_{2d}(/C_1)$ are listed in the subduction diagram (Fig. 19).

It should be pointed out that \mathcal{R}_1 (or \mathcal{R}_4) shown in Fig. 22 is closely related to the segmentation pattern 20 shown in Fig. 8 and that \mathcal{R}_2 (or \mathcal{R}_3) shown in Fig. 22 is closely related to the segmentation pattern 21 shown in Fig. 8. This close relationship has been discussed in general in Chapter 7 of Fujita's book [12].

7.2 Subduction of CRs

As an example of the subduction of CRs, let us examine the CR $\mathbf{D}_{2d}(/C_s)$ diagrammatically. The transformulas listed in Fig. 9 correspond to the eight symmetry operations of \mathbf{D}_{2d} (eq. 1). In order to restrict the original \mathbf{D}_{2d} -symmetry into $\mathbf{C}_s = \{I, \sigma_{d(1)}\}$ (eq. 7), we select 20 and 25, as shown in Fig. 24. This subduction is designated by the symbol $\mathbf{D}_{2d}(/C_s) \downarrow \mathbf{C}_s$, if we take account of the orbit $\mathcal{A} = \{\mathcal{A}_1, \mathcal{A}_2, \mathcal{A}_3, \mathcal{A}_4\}$.

By the inspection of 20 and 25, the four-membered orbit \mathcal{A} is found to be divided into three orbits, i.e., two one-membered orbits ($\mathcal{A}_\alpha = \{\mathcal{A}_1\}$ and $\mathcal{A}_\beta = \{\mathcal{A}_3\}$) and one two-membered orbit ($\mathcal{A}_\gamma = \{\mathcal{A}_2, \mathcal{A}_4\}$). This process corresponds to the selection of $I \sim (1)(2)(3)(4)$ (eq. 23) and $\sigma_{d(1)} \sim (1)(2\ 4)(4)$ (eq. 27), when we keep in mind the concrete form of $\mathbf{D}_{2d}(/C_s)$ (eqs. 23–30).

Because the local symmetry of the object \mathcal{A}_1 in \mathcal{A}_α (or \mathcal{A}_3 in \mathcal{A}_β) is determined to be \mathbf{C}_s (Fig. 24), the orbit \mathcal{A}_α (or \mathcal{A}_β) is governed by the CR $\mathbf{C}_s(/C_s)$. The orbit \mathcal{A}_γ is determined to be governed by the CR $\mathbf{C}_s(/C_1)$, since the local symmetry is found to be \mathbf{C}_1 . These results can be summarized by the following equation:

$$\mathbf{D}_{2d}(/C_s) \downarrow \mathbf{C}_s = 2\mathbf{C}_s(/C_s) + \mathbf{C}_s(/C_1) \quad (59)$$

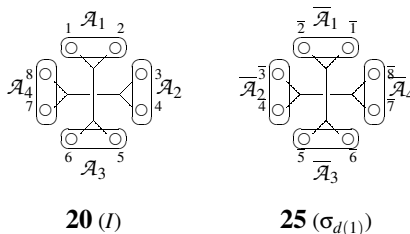


Figure 24: An assembly of two transformulas for the subduction $\mathbf{D}_{2d}(/C_s) \downarrow C_s = 2C_s(/C_s) + C_s(/C_1)$. Thereby, the four-membered orbit \mathcal{A} is divided into two one-membered orbits (i.e., $\mathcal{A}_\alpha = \{\mathcal{A}_1\}$ and $\mathcal{A}_\beta = \{\mathcal{A}_3\}$) and one two-membered orbit (i.e., $\mathcal{A}_\gamma = \{\mathcal{A}_2, \mathcal{A}_4\}$).

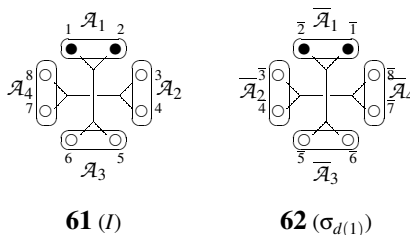


Figure 25: An assembly of two transformulas for an allene derivative generated by the subduction $\mathbf{D}_{2d}(/C_s) \downarrow C_s = 2C_s(/C_s) + C_s(/C_1)$. Thereby, the four-membered orbit \mathcal{A} is divided into two one-membered orbits (i.e., $\mathcal{A}_\alpha = \{\mathcal{A}_1\}$ and $\mathcal{A}_\beta = \{\mathcal{A}_3\}$) and one two-membered orbit (i.e., $\mathcal{A}_\gamma = \{\mathcal{A}_2, \mathcal{A}_4\}$).

The subduction process shown in Fig. 24 allows us to generate C_s -transformulas. For example, the substitution of \mathcal{A}_1 shown in Fig. 25 generates **61** and **62**, as shown in Fig. 23. The resulting transformulas (**61** and **62**) are identical with each other when the numbering is disregarded so that they indicate the occurrence of a single C_s -molecule (**47** or **57**) of this type, which has already been studied in Figs. 20 and 21. In other words, the assembly of the two transformulas (**61** and **62**) represents a C_s -molecule.

From the eight transformulas listed in Fig. 9, the transformulas corresponding to each of the subgroups (eqs. 1 to 8) are selected to give the counterpart of Fig. 24 (for C_s). By the inspection of the transformulas appearing in the counterpart transformulas for the subgroup, we can find the mode of division of the original $\mathbf{D}_{2d}(/C_s)$ -orbit. Thereby, the corresponding subduction is calculated in a similar way to obtain eq. 59. Thereby, we obtain the following subductions of CRs:

Subduction	Result	USCI-CF	USCI	Mark	
$\mathbf{D}_{2d}(/C_s) \downarrow \mathbf{D}_{2d} = \mathbf{D}_{2d}(/C_s)$		a_4	s_4	0	(60)
$\mathbf{D}_{2d}(/C_s) \downarrow \mathbf{D}_2 = \mathbf{D}_2(/C_1)$		b_4	s_4	0	(61)
$\mathbf{D}_{2d}(/C_s) \downarrow \mathbf{C}_{2v} = \mathbf{C}_{2v}(/C_s) + \mathbf{C}_{2v}(/C'_s)$		a_2^2	s_2^2	0	(62)

$$\mathbf{D}_{2d}(/C_s) \downarrow S_4 = S_4(/C_1) \qquad c_4 \qquad s_4 \qquad 0 \qquad (63)$$

$$\mathbf{D}_{2d}(/C_s) \downarrow C_s = 2C_s(/C_s) + C_s(/C_1) \qquad a_1^2 c_2 \qquad s_1^2 s_2 \qquad 2 \qquad (64)$$

$$\mathbf{D}_{2d}(/C_s) \downarrow C_2 = 2C_2(/C_1) \qquad b_2^2 \qquad s_2^2 \qquad 0 \qquad (65)$$

$$\mathbf{D}_{2d}(/C_s) \downarrow C'_2 = 2C'_2(/C_1) \qquad b_2^2 \qquad s_2^2 \qquad 0 \qquad (66)$$

$$\mathbf{D}_{2d}(/C_s) \downarrow C_1 = 4C_1(/C_1) \qquad b_1^4 \qquad s_1^4 \qquad 4 \qquad (67)$$

The results shown in eqs. 60–67 correspond to the subduction diagram shown in Fig. 21, although it contains USCI-CFs (and USCIs) only.

To obtain eq. 59 diagrammatically, Fig. 24 is used as a key, which is based on the concept of *segmentation-pattern superposition*. Note that Fig. 24 is obtained from Fig. 9, which is in turn regarded as the superposition of the transformula **20** (Fig. 8) onto Fig. 7. Similarly, in order to obtain the counterparts of Fig. 24 for the subduction of other CRs, the transformula **20** (Fig. 8) for $\mathbf{D}_{2d}(/C_s) \downarrow C_s$ is replaced by **29** (Fig. 10) for $\mathbf{D}_{2d}(/C'_2) \downarrow C_s$, **31** (Fig. 11) for $\mathbf{D}_{2d}(/C_2) \downarrow C_s$, **32** (Fig. 12) for $\mathbf{D}_{2d}(/C_{2v}) \downarrow C_s$, **33** (Fig. 13) for $\mathbf{D}_{2d}(/D_2) \downarrow C_s$, and **34** (Fig. 14) for $\mathbf{D}_{2d}(/S_4) \downarrow C_s$. Thereby, respective segmentation-pattern superpositions give the following results diagrammatically:

Subduction	Result	USCI-CF	USCI	Mark	
$\mathbf{D}_{2d}(/C'_2) \downarrow C_s = 2C_s(/C_1)$		c_2^2	s_2^2	0	(68)
$\mathbf{D}_{2d}(/C_2) \downarrow C_s = 2C_s(/C_1)$		c_2^2	s_2^2	0	(69)
$\mathbf{D}_{2d}(/C_{2v}) \downarrow C_s = 2C_s(/C_s)$		a_1^2	s_1^2	2	(70)
$\mathbf{D}_{2d}(/D_2) \downarrow C_s = C_s(/C_1)$		c_2	s_2	0	(71)
$\mathbf{D}_{2d}(/S_4) \downarrow C_s = C_s(/C_1)$		c_2	s_2	0	(72)

Exercise 21. From the transformulas listed in Fig. 7, select transformulas corresponding to each subgroup (G_j , cf. eq. 9) to generate such an assembly as shown Fig. 22. Use a segmentation pattern for a CR $\mathbf{D}_{2d}(/G_i)$ (i.e., **29** (Fig. 10) for $\mathbf{D}_{2d}(/C'_2)$, **31** (Fig. 11) for $\mathbf{D}_{2d}(/C_2)$, **32** (Fig. 12) for $\mathbf{D}_{2d}(/C_{2v})$, **33** (Fig. 13) for $\mathbf{D}_{2d}(/D_2)$, or **34** (Fig. 14) for $\mathbf{D}_{2d}(/S_4)$) in place of **20** (Fig. 8) for $\mathbf{D}_{2d}(/C_s)$. Superpose the segmentation pattern onto the assembly so as to generate an segmented assembly (e.g., Fig. 24), which gives the subduction represented by the $\mathbf{D}_{2d}(/G_i) \downarrow G_j$. For the results, see Table 8.

7.3 Tables for the USCI approach

7.3.1 Subduction Tables

The results obtained in the preceding subsection is summarized as a tabular form called a *subduction table*, as shown in Table 8, where eqs. 60–67 appear in the $\mathbf{D}_{2d}(/C_s)$ -row and eqs. 68–72 appear in the $\downarrow C_s$ -column. Similarly, subduction tables for other point groups can be obtained.

It should be emphasized here that Table 8 has been diagrammatically obtained by following the procedure described above. Subduction tables for representative point groups are also obtained algebraically and collected in the Appendix of Fujita's book [12].

7.3.2 USCI-CF Tables

The subduction data shown in eqs. 60–67 and eqs. 68–72 can be easily translated into the corresponding USCI-CFs, which are products of sphericity indices based on the criteria shown in

Table 8: Subduction Table for \mathbf{D}_{2d} [12]

	$\downarrow C_1$	$\downarrow C_2$	$\downarrow C_2'$	$\downarrow C_s$	$\downarrow S_4$	$\downarrow C_{2v}$	$\downarrow D_2$	$\downarrow D_{2d}$
$\mathbf{D}_{2d}/(C_1)$	$8C_1/(C_1)$	$4C_2/(C_1)$	$4C_2'/(C_1)$	$4C_s/(C_1)$	$2S_4/(C_1)$	$2C_{2v}/(C_1)$	$2D_2/(C_1)$	$D_{2d}/(C_1)$
$\mathbf{D}_{2d}/(C_2)^*$	$4C_1/(C_1)$	$4C_2/(C_2)$	$2C_2'/(C_1)$	$2C_s/(C_1)$	$2S_4/(C_2)$	$2C_{2v}/(C_2)$	$2D_2/(C_2)$	$D_{2d}/(C_2)$
$\mathbf{D}_{2d}/(C_2')$	$4C_1/(C_1)$	$2C_2/(C_1)$	$C_2/(C_1)$ $+2C_2'/(C_2')$	$2C_s/(C_1)$	$S_4/(C_1)$	$C_{2v}/(C_1)$	$D_2/(C_2')$ $+D_2/(C_2')$	$D_{2d}/(C_2')$
$\mathbf{D}_{2d}/(C_s)$	$4C_1/(C_1)$	$2C_2/(C_1)$	$2C_2'/(C_1)$	$C_s/(C_1)$ $+2C_s/(C_s)$	$S_4/(C_1)$	$C_{2v}/(C_s)$ $+C_{2v}/(C_s')$	$D_2/(C_1)$	$D_{2d}/(C_s)$
$\mathbf{D}_{2d}/(S_4)^*$	$2C_1/(C_1)$	$2C_2/(C_2)$	$C_2'/(C_1)$	$C_s/(C_1)$	$2S_4/(S_4)$	$C_{2v}/(C_2)$	$D_2/(C_2)$	$D_{2d}/(S_4)$
$\mathbf{D}_{2d}/(C_{2v})$	$2C_1/(C_1)$	$2C_2/(C_2)$	$C_2'/(C_1)$	$2C_s/(C_s)$	$S_4/(C_2)$	$2C_{2v}/(C_{2v})$	$2D_2/(C_2)$	$D_{2d}/(C_{2v})$
$\mathbf{D}_{2d}/(D_2)^*$	$2C_1/(C_1)$	$2C_2/(C_2)$	$2C_2'/(C_2)$	$C_s/(C_1)$	$S_4/(C_2)$	$C_{2v}/(C_2)$	$2D_2/(D_2)$	$D_{2d}/(D_2)$
$\mathbf{D}_{2d}/(D_{2d})$	$C_1/(C_1)$	$C_2/(C_2)$	$C_2'/(C_2')$	$C_s/(C_s)$	$S_4/(S_4)$	$C_{2v}/(C_{2v})$	$D_2/(D_2)$	$D_{2d}/(D_{2d})$

* Forbidden CR. See Chapter 7 of Fujita's book [12].

Table 5. Obviously, the whole data collected in the subduction table (Table 8) can be converted into USCI-CFs, which construct a USCI-CF table, as shown in Table 9.

Table 9: USCI-CF Table for \mathbf{D}_{2d} [12]

	$\downarrow C_1$	$\downarrow C_2$	$\downarrow C_2'$	$\downarrow C_s$	$\downarrow S_4$	$\downarrow C_{2v}$	$\downarrow D_2$	$\downarrow D_{2d}$
$\mathbf{D}_{2d}/(C_1)$	b_1^8	b_2^4	b_2^4	c_2^4	c_4^4	c_4^2	b_4^4	c_8
$\mathbf{D}_{2d}/(C_2)$	b_1^4	b_1^4	b_2^2	c_2^2	c_2^2	c_2^2	b_2^2	c_4
$\mathbf{D}_{2d}/(C_2')$	b_1^4	b_2^2	$b_1^2 b_2$	c_2^2	c_4	c_4	b_2^2	c_4
$\mathbf{D}_{2d}/(C_s)$	b_1^4	b_2^2	b_2^2	$a_1^2 c_2$	c_4	a_2^2	b_4	a_4
$\mathbf{D}_{2d}/(S_4)$	b_1^2	b_1^2	b_2	c_2	a_1^2	c_2	b_2	a_2
$\mathbf{D}_{2d}/(C_{2v})$	b_1^2	b_1^2	b_2	a_1^2	c_2	a_1^2	b_2	a_2
$\mathbf{D}_{2d}/(D_2)$	b_1^2	b_1^2	b_1^2	c_2	c_2	c_2	b_1^2	c_2
$\mathbf{D}_{2d}/(D_{2d})$	b_1	b_1	b_1	a_1	a_1	a_1	b_1	a_1
$\sum_{i=1}^s \bar{m}_{ji}$	1/8	1/8	1/4	1/4	1/4	0	0	0

It is worthy to remember that the USCI-CFs appearing in eqs. 60–67 (and in the $\mathbf{D}_{2d}/(C_s)$ -row of Table 9) have been already discussed in Fig. 3. This means that the USCI-CFs obtained diagrammatically from Tables 3 and 4 are equivalent to the USCI-CFs obtained diagrammatically from Figs. 9 and 24. In other words, the orbit of the four hydrogen atoms in **1** (Fig. 3) is symmetrically equivalent to the orbit $\mathcal{A} = \{\mathcal{A}_1, \mathcal{A}_2, \mathcal{A}_3, \mathcal{A}_4\}$ in Fig. 9.

Such USCI-CF tables for representative point groups are also obtained algebraically and collected in the Appendix of Fujita's book [12].

7.3.3 USCI Tables

The USCI-CFs derived from the subduction data (eqs. 60–67 and eqs. 68–72) can be further translated into the corresponding USCIs, where the sphericity indices of three kinds ($a_d, c_d,$

and b_d) are replaced by a single dummy variable s_d . Obviously, the whole data collected in the USCI-CF table (Table 9) can be converted into USCIs, which construct the USCI table, as shown in Table 10.

Table 10: USCI Table for \mathbf{D}_{2d} [12]

	$\downarrow C_1$	$\downarrow C_2$	$\downarrow C_2'$	$\downarrow C_s$	$\downarrow S_4$	$\downarrow C_{2v}$	$\downarrow D_2$	$\downarrow D_{2d}$
$\mathbf{D}_{2d}/(C_1)$	s_1^8	s_2^4	s_2^4	s_2^4	s_4^2	s_4^2	s_4^2	s_8
$\mathbf{D}_{2d}/(C_2)$	s_1^4	s_1^4	s_2^2	s_2^2	s_2^2	s_2^2	s_2^2	s_4
$\mathbf{D}_{2d}/(C_2')$	s_1^4	s_2^2	$s_1^2 s_2$	s_2^2	s_4	s_4	s_2^2	s_4
$\mathbf{D}_{2d}/(C_s)$	s_1^4	s_2^2	s_2^2	$s_1^2 s_2$	s_4	s_2^2	s_4	s_4
$\mathbf{D}_{2d}/(S_4)$	s_1^2	s_1^2	s_2	s_2	s_1^2	s_2	s_2	s_2
$\mathbf{D}_{2d}/(C_{2v})$	s_1^2	s_1^2	s_2	s_1^2	s_2	s_1^2	s_2	s_2
$\mathbf{D}_{2d}/(D_2)$	s_1^2	s_1^2	s_1^2	s_2	s_2	s_2	s_1^2	s_2
$\mathbf{D}_{2d}/(D_{2d})$	s_1	s_1	s_1	s_1	s_1	s_1	s_1	s_1
$\sum_{i=1}^s \bar{m}_{ji}$	1/8	1/8	1/4	1/4	1/4	0	0	0

Such USCI tables for representative point groups are also obtained algebraically and collected in the Appendix of Fujita's book [12].

7.3.4 Mark Tables

The concept of *marks*, which was originally proposed by Burnside in 1911 [35], has long been forgotten even in mathematical fields, even though several pioneering works [36, 37] appeared to describe applications of the concept. The USCI approach described in Fujita's book [12] has vitalized the concept of marks, which has been further combined with the concept of CRs.⁸ Thereby, the USCI approach has developed several new concepts, i.e., sphericities of CRs, sphericity indices, subduction of CRs, USCIs, USCI-CFs, etc., which have been further used to develop a new theoretical framework for discussing intramolecular stereochemistry, stereoisomerism (intermolecular stereochemistry), and chemical combinatorics.

As found in the preceding paragraph, in the original formulation of the USCI approach, marks have been obtained by algebraic procedures and collected in the Appendix of Fujita's book [12].

Because a mark is the number of fixed elements (objects), such marks can be easily obtained by starting from the data of USCI-CFs (or USCIs). That is to say, the mark is equal to the sum of the powers of sphericity indices for one-membered orbits, i.e., a_1 and b_1 (or s_1). For example, the USCI-CFs data shown in eqs. 60–67 and eqs. 68–72 give the corresponding marks, as shown in the end of each equation. Obviously, the whole data collected in the USCI-CF table (Table 9) or the USCI table (Table 10) can be converted into marks, which construct a mark table, as shown in Table 11.

⁸One of the most essential points of the USCI approach is the explicit recognition of the fact that two or more mark tables are nested to characterize group-subgroup relationships. This point has been discussed in terms of *subduced mark tables* in Chapter 9 of Fujita's book.

Table 11: Mark Table for \mathbf{D}_{2d} [12]

	\mathbf{C}_1	\mathbf{C}_2	\mathbf{C}'_2	\mathbf{C}_s	\mathbf{S}_4	\mathbf{C}_{2v}	\mathbf{D}_2	\mathbf{D}_{2d}
$\mathbf{D}_{2d}/(\mathbf{C}_1)$	8	0	0	0	0	0	0	0
$\mathbf{D}_{2d}/(\mathbf{C}_2)$	4	4	0	0	0	0	0	0
$\mathbf{D}_{2d}/(\mathbf{C}'_2)$	4	0	2	0	0	0	0	0
$\mathbf{D}_{2d}/(\mathbf{C}_s)$	4	0	0	2	0	0	0	0
$\mathbf{D}_{2d}/(\mathbf{S}_4)$	2	2	0	0	2	0	0	0
$\mathbf{D}_{2d}/(\mathbf{C}_{2v})$	2	2	0	2	0	2	0	0
$\mathbf{D}_{2d}/(\mathbf{D}_2)$	2	2	2	0	0	0	2	0
$\mathbf{D}_{2d}/(\mathbf{D}_{2d})$	1	1	1	1	1	1	1	1

7.3.5 Comparison between the Tables

As summarized in Tables 8–11, each orbit is characterized in different ways by the data generated during symmetry restriction into subgroups, i.e., its subduction data, its USCI-CFs, its USCIs, and its marks. For example, the $\mathbf{D}_{2d}/(\mathbf{C}_s)$ -orbit is characterized by the subductions (eqs. 60–67), by the USCI-CFs ($\{b_1^4, b_2^2, b_2^2, a_1^2 c_2, c_4, a_2^2, b_4, a_4\}$), by the USCIs ($\{s_1^4, s_2^2, s_2^2, s_1^2 s_2, s_4, s_2^2, s_4, s_4\}$), and by the marks ($\{4, 0, 0, 2, 0, 0, 0, 0, 0\}$), where these are aligned in an ascending order of the orders of the subgroups (cf. the $\mathbf{D}_{2d}/(\mathbf{C}_s)$ -rows of Tables 8–10).

As found easily, subduction tables are more informative than USCI-CF tables because the former can generate the latter but the reverse procedure is impossible without other information. The data of global and local symmetries are lost during the process of converting the subduction tables into the USCI-CF tables. The USCI-CF tables are, in turn, more informative than USCI tables because the former can generate the latter but the reverse is impossible without other information. The data of sphericities are lost during the process of converting the USCI-CF tables into the USCI tables. Moreover, the USCI tables are, in turn, more informative than mark tables because the former can generate the latter but the reverse is impossible without other information.⁹

In the present diagrammatical USCI approach, necessary tables (i.e., subduction tables, USCI-CF tables, USCI tables, and mark tables) are obtained *diagrammatically* without considering concrete forms of CRs. Thus, subduction tables are obtained by comparing a global symmetry (\mathbf{G}) with a local symmetry (\mathbf{H}) during desymmetrization processes; USCI-CF tables are obtained in terms of the criteria listed in Tables 1 and 2 or by extracting necessary data from subduction tables; and mark tables are obtained by counting fixed objects or by extracting necessary data from USCI-CF tables.

7.3.6 Mathematical vs. Diagrammatical Approach

In the original formulation of Fujita’s USCI approach [12], the mark tables of a group \mathbf{G} and its subgroup \mathbf{H} are used to obtain subduction tables and USCI-CF tables, where concrete forms

⁹The other information necessary to reversely generate subduction data is concerned with the mark tables of subgroups. The nested nature of these mark tables is a foundation of Fujita’s USCI approach (cf. Chapter 9 of Fujita’s book [12]).

of CRs are taken into consideration to count fixed objects. This mathematical feature would be a reason to bring about "an organic chemistry paradox". However, the USCI approach has, in fact, applied the resulting tables to diagrammatical studies on intra- and intermolecular stereochemistries, although the details of the diagrammatical studies have not always been described in Fujita's book [12]. Hence, such diagrammatical data as omitted for the sake of compactness of the book would be still valuable if they are systematized to support graduate students and their teachers. Thus, the present diagrammatical approach is an explicit version of the diagrammatical methodology that has been implicitly involved in the original algebraic USCI approach.

Although the diagrammatical USCI approach is sufficient and useful to chemical applications, the original algebraic USCI approach is necessary to more detailed discussions on stereochemistry. Hence, the diagrammatical USCI approach should be correlated to the algebraic USCI approach in a more explicit fashion. The next section is devoted to this task.

8 Diagrammatical Correspondence Between Segments and Cosets

As discussed in Chapter 5 of Fujita's book [12], the essence of the USCI approach can be stated: "Each orbit is governed by a coset representation (CR)". This statement will be confirmed diagrammatically in this section.

8.1 Diagrammatical Correspondence Between Positions of a Regular Body and Symmetry Operations

Although the subject at issue has been described in a previous paper [38], it will be treated more diagrammatically from a viewpoint of concurrent controls of CRs.

Let us first study the regular representation $\mathbf{D}_{2d}(/C_1)$ as an extreme case of CRs. The eight positions of a regular body of \mathbf{D}_{2d} is related to the symmetry operations of \mathbf{D}_{2d} in one-to-one correspondence:

$$\begin{array}{cccccccc} \mathcal{R} & = & \{ & 1, & 2, & 3, & 4, & 5, & 6, & 7, & 8 & \} \\ & & & \updownarrow & \updownarrow & \updownarrow & \updownarrow & \updownarrow & \updownarrow & \updownarrow & \updownarrow & \\ \mathbf{D}_{2d} & = & \{ & I, & \sigma_{d(1)}, & S_4, & C_{2(1)}, & C_{2(3)}, & \sigma_{d(2)}, & S_4^3, & C_{2(2)} & \} \end{array} \quad (73)$$

For example, because the position 1 ($\leftrightarrow I$) is moved to the position 5 by $C_{2(3)}$, the position 5 is regarded as corresponding to the symmetry operation $C_{2(3)}$. This procedure is repeated to cover all of the symmetry operations of \mathbf{D}_{2d} (eq. 1). Thereby, the correspondence (eq. 73) is diagrammatically represented by the transformula **63** shown in Fig. 26.¹⁰

By keeping the correspondence (eq. 73) in mind, we find that the operation of $C_{2(3)}$ onto the transformula **63** gives another transformula **64**. Because this operation is essentially equivalent to the one onto **11** (Fig. 7), the same permutation as represented by eq. 15 is assigned to the operation $C_{2(3)}$. Moreover, the correspondence represented by eq. 73 generates a permutation of symmetry operations according to the multiplication of symmetry operations. Thereby, we obtain the following correspondence:

¹⁰In general, the numbering of symmetry operations can be selected arbitrarily in eq. 73. In this case, however, it is determined in one-to-one fashion because the numbering of positions has already been fixed and the correspondence $I \leftrightarrow 1$ is presumed.

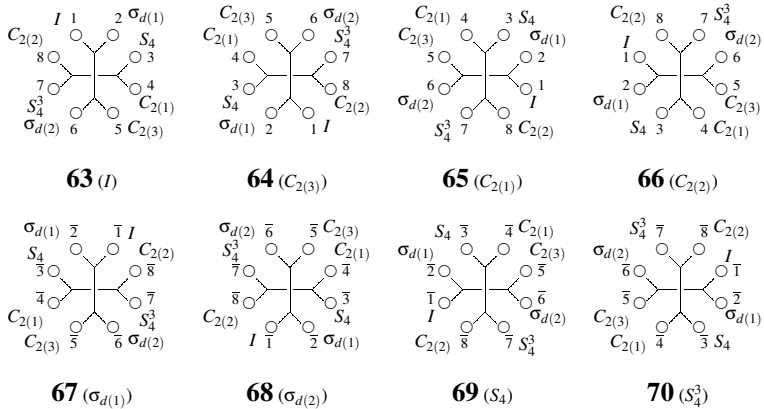


Figure 26: Diagrammatic correspondence between symmetry operations and the positions of the regular body of D_{2d} (**63**), generating the regular representation (D_{2d}/C_1)).

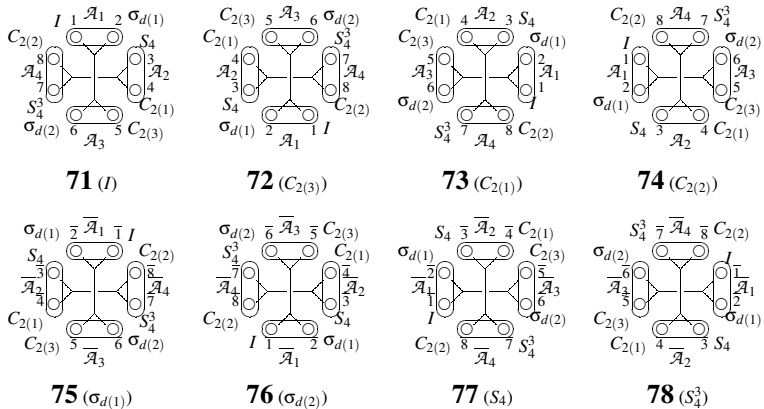


Figure 27: Diagrammatic correspondence between the set of cosets (D_{2d}/C_s) and the set the C_s -segments ($\mathcal{A} = \{\mathcal{A}_1, \mathcal{A}_2, \mathcal{A}_3, \mathcal{A}_4\}$) in the regular body of D_{2d} (**71**), generating the CR D_{2d}/C_s . This diagram is generated by superposing Fig. 8 onto Fig. 26.

$$\begin{aligned}
 C_{2(3)} &\sim \begin{pmatrix} I & \sigma_{d(1)} & S_4 & C_{2(1)} & C_{2(3)} & \sigma_{d(2)} & S_4^3 & C_{2(2)} \\ C_{2(3)} & \sigma_{d(2)} & S_4^3 & C_{2(2)} & I & \sigma_{d(1)} & S_4 & C_{2(1)} \end{pmatrix} \\
 &\sim \begin{pmatrix} 1 & 2 & 3 & 4 & 5 & 6 & 7 & 8 \\ 5 & 6 & 7 & 8 & 1 & 2 & 3 & 4 \end{pmatrix} = (1\ 5)(2\ 6)(3\ 7)(4\ 8) \quad (74)
 \end{aligned}$$

which is a permutation involved in \mathbf{D}_{2d}/C_1 defined mathematically [12]. Similarly, every symmetry operations onto **63** generate the transformulas **63–70**, which correspond to the permutations listed in eqs. 14–21.

8.2 Diagrammatical Correspondence Between Segments of a Regular Body and Cosets

The symmetry operations of \mathbf{D}_{2d} are categorized into cosets, which are generated by the coset decomposition of \mathbf{D}_{2d} by a subgroup (e.g., C_s) as follows:

$$\mathbf{D}_{2d} = IC_s + C_{2(3)}C_s + C_{2(1)}C_s + C_{2(2)}C_s \quad (75)$$

$$= \underbrace{\{I, \sigma_{d(1)}\}}_{\mathcal{M}_1} + \underbrace{\{C_{2(3)}, \sigma_{d(2)}\}}_{\mathcal{M}_3} + \underbrace{\{C_{2(1)}, S_4\}}_{\mathcal{M}_2} + \underbrace{\{C_{2(2)}, S_4^3\}}_{\mathcal{M}_4} \quad (76)$$

Let us regard these cosets as an ordered set:

$$\mathbf{D}_{2d}/C_s = \{\mathcal{M}_1, \mathcal{M}_2, \mathcal{M}_3, \mathcal{M}_4\} \quad (77)$$

The ordered set \mathbf{D}_{2d}/C_s gives the CR \mathbf{D}_{2d}/C_s as a permutation representation. This is a mathematical formulation which the USCI approach relies on [12].

The mathematical formulation of CRs can be correlated to the diagrammatical formulation described above. Let us superpose the segmentation pattern shown in Fig. 8 onto Fig. 26. Then, we can obtain Fig. 27, which is essentially equivalent to Fig. 9. By inspection of **71** in Fig. 27, we have the following correspondence between the orbit of segments \mathcal{A} and the set of cosets \mathbf{D}_{2d}/C_s :

$$\begin{aligned}
 \mathcal{A} &= \left\{ \begin{array}{cccc} \mathcal{A}_1, & \mathcal{A}_2, & \mathcal{A}_3, & \mathcal{A}_4 \\ \{1, 2\} & \{3, 4\} & \{5, 6\} & \{7, 8\} \end{array} \right\} \\
 &\quad \downarrow \qquad \downarrow \qquad \downarrow \qquad \downarrow \\
 \mathbf{D}_{2d}/C_s &= \left\{ \begin{array}{cccc} \{I, \sigma_{d(1)}\} & \{S_4, C_{2(1)}\} & \{C_{2(3)}, \sigma_{d(2)}\} & \{S_4^3, C_{2(2)}\} \\ \mathcal{M}_1, & \mathcal{M}_2, & \mathcal{M}_3, & \mathcal{M}_4 \end{array} \right\} \quad (78)
 \end{aligned}$$

The operation of $C_{2(3)}$ onto the transformula **71** gives another transformula **72** by taking account of the correspondence (eq. 78). Because this operation is essentially equivalent to the one onto **20** (Fig. 9), the same permutation as represented by eq. 24 is assigned to the operation $C_{2(3)}$. Moreover, the correspondence represented by eq. 78 generates a permutation of the set of cosets (\mathbf{D}_{2d}/C_s). Thereby, we obtain the following correspondence:

$$\begin{aligned}
 C_{2(3)} &\sim \begin{pmatrix} \mathcal{A}_1 & \mathcal{A}_2 & \mathcal{A}_3 & \mathcal{A}_4 \\ \mathcal{A}_3 & \mathcal{A}_4 & \mathcal{A}_1 & \mathcal{A}_2 \end{pmatrix} \\
 &\sim \begin{pmatrix} \mathcal{M}_1 & \mathcal{M}_2 & \mathcal{M}_3 & \mathcal{M}_4 \\ \mathcal{M}_3 & \mathcal{M}_4 & \mathcal{M}_1 & \mathcal{M}_2 \end{pmatrix} \\
 &\sim \begin{pmatrix} 1 & 2 & 3 & 4 \\ 3 & 4 & 1 & 2 \end{pmatrix} = (1\ 3)(2\ 4), \quad (79)
 \end{aligned}$$

which is a permutation involved in $\mathbf{D}_{2d}/\langle \mathbf{C}_s \rangle$ defined mathematically [12]. Similarly, every symmetry operations onto **71** generate the transformulas **71–78**, which correspond to the permutations listed in eqs. 23–30.

The importance of eqs. 78 and 79 cannot be overstated although it has a simple form. Thus, the orbit \mathcal{A} (the orbit of segments) corresponds to the orbit $\mathbf{D}_{2d}/\mathbf{C}_s$ (the orbit of cosets) in one-to-one fashion so that both the orbits of different kinds are concurrently governed by the CR $\mathbf{D}_{2d}/\langle \mathbf{C}_s \rangle$. This feature has been discussed in general and mathematically in Chapter 7 of Fujita's book (especially see Fig. 7.1) [12]. Because eq. 79 is accompanied by a diagrammatical expression (Fig. 27), the correspondence provides us with versatile tools for comprehending intramolecular stereochemistry, i.e., the tools developed by the USCI approach [12].

The procedure described above for the superposition of Fig. 8 onto Fig. 26 (for \mathbf{C}_s -segments) can be generally applied to the other modes of segmentation. In place of Fig. 8, we superpose Fig. 10 (for \mathbf{C}'_2 -segments), Fig. 11 (for \mathbf{C}_2 -segments), Fig. 12 (for \mathbf{C}_{2v} -segments), Fig. 13 (for \mathbf{D}_2 -segments), or Fig. 14 (for \mathbf{S}_4 -segments) onto Fig. 26 so as to obtain the corresponding diagrammatical expression similar to Fig. 27. The exercises concerning the other modes of segmentation challenge the reader to comprehend the importance of the concurrent features of CRs.

8.3 Subduction of CRs and Double Cosets

The relationship between subduction of coset representations and double cosets has been discussed in general [39]. When the group \mathbf{G} is decomposed into the following double coset decomposition:

$$\mathbf{G} = \mathbf{G}_j g'_1 \mathbf{G}_i + \mathbf{G}_j g'_2 \mathbf{G}_i + \cdots + \mathbf{G}_j g'_r \mathbf{G}_i, \quad (80)$$

where the transversal is placed as follows:

$$\Upsilon = \{g'_1, g'_2, \dots, g'_r\} \quad (81)$$

Then, Theorem 2 of Ref. [39] teaches us as follows:

$$\mathbf{G}/\langle \mathbf{G}_i \rangle \downarrow \mathbf{G}_j = \sum_{g \in \Upsilon} \mathbf{G}_j \langle g \mathbf{G}_i g^{-1} \cap \mathbf{G}_j \rangle \quad (82)$$

Note that $g \mathbf{G}_i g^{-1}$ which is conjugate to \mathbf{G}_i is the stabilizer of the coset $g \mathbf{G}_i$. The integer $|\mathbf{G}_j|/|g \mathbf{G}_i g^{-1} \cap \mathbf{G}_j|$ derived from the right-hand side of eq. 82 represents the number of cosets in the double coset $\mathbf{G}_j g \mathbf{G}_i$ ($g \in \Upsilon$). This means that several cosets $g \mathbf{G}_i$ are fused under the action of \mathbf{G}_j into a double coset to satisfy eq. 82. This process of fusion can be modelled by the concept of doubly-colored graphs, as shown in a previous paper [31].

This process of fusion can be alternatively explained by the superposition of the segmentation pattern described above. For example, by selecting **63** and **67** according to the subgroup \mathbf{C}_s , Fig. 28 is obtained to represent the subduction $\mathbf{D}_{2d}/\langle \mathbf{C}_1 \rangle \downarrow \mathbf{C}_s$ diagrammatically. The comparison between **63** and **67** shows that this subduction divides the eight positions into four two-membered orbits, i.e., $\{1, 2\}$, $\{3, 8\}$, $\{4, 7\}$, and $\{5, 6\}$. By inspection of **63** or **67**, these sets correspond to the following sets of (left) cosets: $\{I, \sigma_{d(1)}\}$ $\{S_4, C_{2(2)}\}$ $\{C_{2(1)}, S_4^3\}$, and $\{C_{2(3)}, \sigma_{d(2)}\}$.

The symmetry operations of \mathbf{D}_{2d} are categorized into (right) cosets, which are generated by the (right) coset decomposition of \mathbf{D}_{2d} by a subgroup (e.g., \mathbf{C}_s). Strictly speaking, the

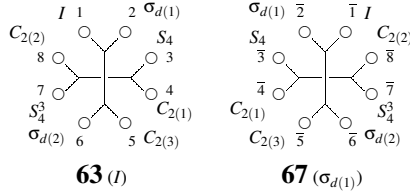


Figure 28: An Assembly of transformulas for representing the subduction $\mathbf{D}_{2d}(/C_1) \downarrow C_s = 4C_s(/C_1)$.

subduction is concerned with a double coset decomposition as follows:¹¹

$$\begin{aligned} \mathbf{D}_{2d} &= C_s I C_1 + C_s C_{2(2)} C_1 + C_s C_{2(1)} C_1 + C_s C_{2(3)} C_1 \\ &= \underbrace{\{I, \sigma_{d(1)}\}}_{\{1,2\}} + \underbrace{\{S_4, C_{2(2)}\}}_{\{3,8\}} + \underbrace{\{C_{2(1)}, S_4^3\}}_{\{4,7\}} + \underbrace{\{C_{2(3)}, \sigma_{d(2)}\}}_{\{5,6\}} \end{aligned} \quad (83)$$

Because of $gC_1g^{-1} \cap C_s = C_1$, eq. 82 for this case is obtained as follows:

$$\mathbf{D}_{2d}(/C_1) \downarrow C_s = 4C_s(/C_1), \quad (84)$$

which is a special case of eq. 58, although the derivation method of this equation is different from that of eq. 58.

By selecting **71** and **75** according to the subgroup C_s , Fig. 29 is obtained to represent the subduction $\mathbf{D}_{2d}(/C_s) \downarrow C_s$ diagrammatically. This diagram is essentially equivalent to Fig. 24 except the correspondence between the positions and the symmetry operations of \mathbf{D}_{2d} . The comparison between **71** and **75** shows that this subduction divides the set of segments ($\mathcal{A} = \{\mathcal{A}_1, \mathcal{A}_2, \mathcal{A}_3, \mathcal{A}_4\}$) into three orbits, i.e., $\{\mathcal{A}_1\}$, $\{\mathcal{A}_2, \mathcal{A}_4\}$, and $\{\mathcal{A}_3\}$. By inspection of **71** or **75**, these sets correspond to the following sets: $\{I, \sigma_{d(1)}\}$ (stabilizer: C_s), $\{S_4, C_{2(1)}\}$, $\{S_4^3, C_{2(2)}\}$ (stabilizer: $C_{2(2)}^{-1} C_s C_{2(2)} = C'_s$), and $\{C_{2(3)}, \sigma_{d(2)}\}$ (stabilizer: $C_{2(3)}^{-1} C_s C_{2(3)} = C_s$). Following the general treatment described in [39], the resulting sets correspond to the double coset decomposition represented by the following equation:

$$\begin{aligned} \mathbf{D}_{2d} &= C_s I C_s + C_s C_{2(1)} C_s + C_s C_{2(3)} C_s \\ &= \underbrace{\{I, \sigma_{d(1)}\}}_{\{1,2\}} + \underbrace{\{C_{2(1)}, S_4, \{S_4^3, C_{2(2)}\}\}}_{\{\{3,4\}, \{7,8\}\}} + \underbrace{\{C_{2(3)}, \sigma_{d(2)}\}}_{\{5,6\}} \end{aligned} \quad (85)$$

Because the corresponding stabilizers are calculated to be C_s and C'_s as shown above, the local symmetries appearing in eq. 82 are determined to be $C_s \cap C_s = C_s$ and $C'_s \cap C_s = C_1$. Hence, eq. 82 for this case is obtained as follows:

$$\mathbf{D}_{2d}(/C_s) \downarrow C_s = 2C_s(/C_s) + C_s(/C_1) \quad (86)$$

This is identical with eq. 59, which is obtained by the subduction of CRs.

¹¹By inspection of a double coset $G_j g G_i$ contained in eq. 82, one can find that a (left) coset $g G_i$ is concerned with G_i -segments. On the other hand, G_j is concerned with the precess of subduction (e.g., C_s of eq. 83) as well as with the process of constructing assemblies of transformulas (see Part 2). According to this methodology, each transformula of Fig. 26 corresponds to each of the (left) cosets represented by $\mathbf{D}_{2d} = I C_1 + C_{2(3)} C_1 + \dots + S_4 C_1$.

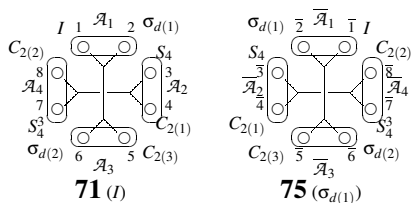


Figure 29: An assembly of transformulas for representing the subduction $\mathbf{D}_{2d}(/C_s) \downarrow C_s = 2C_s(/C_s) + C_s(/C_1)$.

9 Conclusions

The versatility of Fujita's USCI approach (S. Fujita, "Symmetry and Combinatorial Enumeration in Chemistry", Springer-Verlag, 1991) is demonstrated diagrammatically on the basis of orbits as sets of symmetry-equivalent objects. By emphasizing the concurrent appearance and desymmetrization of various orbits, the following items are studied diagrammatically:

1. Any orbits are shown to be controlled by three kinds of sphericity indices (a_d , c_d , and b_d) correlated to coset representations (CRs).
2. Derivation of molecules of given symmetries is discussed in terms of USCI-CFs (unit subduced cycle indices with chirality fittingness), which are obtained diagrammatically as products of sphericity indices.
3. The concurrent behaviors of orbits are explained by using a regular body, the positions of which are segmented in terms of segmentation patterns so as to give segmented regular bodies.
4. Such segments are studied as models of ligands or proligands so that segmented regular bodies can be regarded as models of three-dimensional molecules (stereoisomers).
5. The segmented regular bodies are used to generate CRs and to derive subductions of CRs diagrammatically.
6. The generality of the diagrammatical procedure is confirmed to generate the subduction table, the USCI-CF table, the USCI table, and the mark table of \mathbf{D}_{2d} -point group.
7. Diagrammatical correspondence between segments and cosets are examined in detail so that the relationship between subduction of CRs and double Cosets is clearly demonstrated.

It is concluded that *any symmetrical properties appear in regular bodies*. The present paper has demonstrated an explicit and diagrammatical way of revealing stereochemical information concealed in regular bodies through the concepts of coset representations and sphericities. Thereby, Fujita's USCI approach has been provided with succinct but strict foundations for comprehending intramolecular stereochemistry diagrammatically.

References

- [1] Eliel, E. L. (1980) *J. Chem. Educ.* **57**, 52–55.
- [2] Eliel, E. & Wilen, S. H. (1994) *Stereochemistry of Organic Compounds* (John Wiley & Sons, New York).

- [3] Buxton, S. R. & Roberts, S. M. (1996) *Guide to Organic Stereochemistry* (Addison Wesley Longman, New York).
- [4] von Zelewsky, A. (1996) *Stereochemistry of Coordination Compounds* (John Wiley & Sons, Chichester).
- [5] Mislow, K. & Raban, M. (1967) *Top. Stereochem.* **1**, 1–38.
- [6] Mislow, K. & Siegel, J. (1984) *J. Am. Chem. Soc.* **106**, 3319–3328.
- [7] Pólya, G. (1937) *Acta Math.* **68**, 145–254.
- [8] Pólya, G. & Read, R. C. (1987) *Combinatorial Enumeration of Groups, Graphs, and Chemical Compounds* (Springer-Verlag, New York).
- [9] Fujita, S. (2005) *Theor. Chem. Acc.* **113**, 73–79.
- [10] Fujita, S. (2005) *Theor. Chem. Acc.* **113**, 80–86.
- [11] Fujita, S. (1990) *J. Am. Chem. Soc.* **112**, 3390–3397.
- [12] Fujita, S. (1991) *Symmetry and Combinatorial Enumeration in Chemistry* (Springer-Verlag, Berlin-Heidelberg).
- [13] Fujita, S. (2001) *J. Math. Chem.* **30**, 249–270.
- [14] Fujita, S. (1998) *Bull. Chem. Soc. Jpn.* **71**, 1587–1596.
- [15] Fujita, S. (2002) *Chem. Rec.* **2**, 164–176.
- [16] Fujita, S. (2002) *Bull. Chem. Soc. Jpn.* **75**, 1863–1883.
- [17] Mead, C. A. (1992) *J. Am. Chem. Soc.* **114**, 4018–4019.
- [18] El-Basil, S. (2002) *MATCH Commun. Math. Comput. Chem.* **46**, 7–23.
- [19] Fujita, S. (2001) *Computer-Oriented Representation of Organic Reactions* (Yoshioka-Shoten, Kyoto).
- [20] Fujita, S. (2004) *Organic Chemistry of Photography* (Springer-Verlag, Berlin-Heidelberg).
- [21] Fujita, S. (2002) *J. Org. Chem.* **67**, 6055–6063.
- [22] Fujita, S. (2004) *J. Comput. Chem. Jpn.* **3**, 113–120.
- [23] Fujita, S. (2005) *Chem. Educ. J.* **8**, Registration No. 8-8.
- [24] Fujita, S. (2005) *Chem. Educ. J.* **8**, Registration No. 8-9.
- [25] Fujita, S. (1990) *Bull. Chem. Soc. Jpn.* **63**, 315–327.
- [26] Fujita, S. (1990) *Bull. Chem. Soc. Jpn.* **63**, 1876–1883.
- [27] Fujita, S. (1991) *Tetrahedron* **47**, 31–46.
- [28] Fujita, S. (1986) *J. Chem. Educ.* **63**, 744–746.
- [29] Fujita, S. (1990) *J. Math. Chem.* **5**, 121–156.
- [30] Fujita, S. (1990) *Theor. Chim. Acta* **78**, 45–63.
- [31] Fujita, S. & El-Basil, S. (2004) *J. Math. Chem.* **36**, 211–229.
- [32] Fujita, S. (1991) *J. Chem. Inf. Comput. Sci.* **31**, 540–546.
- [33] Fujita, S. (1990) *Bull. Chem. Soc. Jpn.* **63**, 2033–2043.
- [34] Fujita, S. (1989) *Theor. Chim. Acta* **76**, 247–268.
- [35] Burnside, W. (1911) *Theory of Groups of Finite Order* 2nd edn. (Cambridge University Press, Cambridge).
- [36] Sheehan, J. (1968) *Canad. J. Math.* **20**, 1068–1076.
- [37] Mead, C. A. (1987) *J. Amer. Chem. Soc.* **109**, 2130–2137.
- [38] Fujita, S. (1991) *Bull. Chem. Soc. Jpn.* **64**, 3313–3323.
- [39] Fujita, S. (1994) *J. Graph Theory* **18**, 349–371.